Optimal Energy Efficiency of Isolated PAT systems by SEIG Excitation Tuning

João F.P. Fernandes[1*], Modesto Pérez-Sánchez[2], F. Ferreira da Silva[1], P. Amparo López-Jiménez[2], Helena M. Ramos[3], P.J. Costa Branco[1]

[1] IDMEC, Instituto Superior Técnico, Universidade de Lisboa, Lisboa, 1049-001, Portugal; joao.f.p.fernandes@tecnico.ulisboa.pt; francisco.ferreira.silva@tecnico.ulisboa.pt; pbranco@tecnico.ulisboa.pt

[2] Hydraulic and Environmental Engineering Department, Universitat Politècnica de València, Valencia, 46022 Spain; mopesan1@upv.es; palopez@upv.es

[3] Civil Engineering, Architecture and Georesources Department, CERIS, Instituto Superior Técnico, Universidade de Lisboa, Lisboa, 1049-001, Portugal; hramos.ist@gmail.com

[*] Correspondence: joao.f.p.fernandes@tecnico.ulisboa.pt; Tel.: +351 968811445

ABSTRACT

The use of pump working as turbine (PAT) was identified by many researchers as a way to improve the energy efficiency in the water systems. However, the majority of the researches consider the hydraulic machine connected to the electrical grid, which may not fit best when these recovery systems are located in rural or remote areas. To improve the efficiency in these recovery systems for rural areas, this research contributes for a further study and optimization of the off-grid PAT systems with induction generators. The current manuscript proposes a methodology to obtain the best efficiency of the PAT-SEIG (Self-Excited Induction Generator) system when operating under different speeds and loads. For these systems, the selection of capacitors for the SEIG is critical to maximizing the energy efficiency. A methodology is proposed to estimate and select the correct SEIG model parameters and, thus, compute the best capacitor values to improve the PAT-SEIG energy efficiency. Special attention is given to the impact the SEIG parameters have in the efficiency of the recovery system. The accuracy of the analytical model improved, reducing the error between analytical and experimental results from 50.8% (for a model with constant parameters) to 13.2% (with parameters changing according to the operating point of the system). These results showed an increase of the overall PAT system efficiency from 26% to 40% for the analyzed case study.

KEYWORDS: Energy Efficiency; Off-grid PAT; Self-excited Induction Generator (SEIG); water-energy nexus.

1 Introduction

New challenges in the society development are focused on the sustainability reach in all systems [1]. Particularly in the water systems, the search for this sustainability is noticed and the efficiency improvement is one of the water managing system's main goals. Regarding the water management in different supply systems (i.e., urban, industrial or irrigation), the sustainability has been improved by reducing leakages as well as the control by the pressure along the system. The proposal of pumps working as turbines (PATs) to replace to pressure reduction valves (PRVs) is a way to control the pressure [2]-[3]. A case study in Brazil was done by using hydraulic energy recovery was studied in substitution of pressure reduction devices [4]. Previously, Williams proposed the use of the PATs in remote areas in order to generate energy in areas without access to the electrical grid [5]. The proposal for this type of recovery machine led to several studies about the analysis of the hydraulic efficiency of a pump and the behavior on the grid [6]-[7]. Different works analyzed the recovered energy using PATs. The real recovered energy represents up to 5% of the available energy (i.e., the energy that can be leveraged in the system, ensuring the correct operating in terms of pressure in the consumption point. This energy is variable and depends on circulating flow) in a water supply system located in Lausanne (Switzerland) [8]. In Fribourg, the recovered energy reached 10% of the available energy in other water supply system [9]. In Vallada (Spain), the recovered energy represented 9.55% of the provided energy in the network [10]. In the case study developed in Italy, the recovered energy reached 300 MWh/year using recovery machines which had a power of 25 kW [11]. These are examples of the potential of these recovery systems, however, in the majority of them, their operation was off-grid (not connected to the electric grid) and the analysis of the recovery energy did not consider the effect of this operation in the efficiency of the machine, since the majority of PATs manufacturer show the machine efficiency as well as the efficiency of electric motor when it is connected to the grid.

A deep review done in [7] identified the lack of information in the global PAT behavior, considering a symbiosis between electricity and hydraulic aspects when these recovery machines operate in stand-alone [7]-[12]. The "off-grid" operation is crucial since the main goal of this generated energy is to supply low-voltage/low-power consumptions [12]. Increasing the effectiveness of hydraulic energy recovery systems is crucial when those are applied to water distribution networks, which are among the top energy users worldwide. Therefore, although the energy recovery directly depends on the hydraulic conditions, the implication of the electrical parameters is very significant for the global efficiency of the system. The importance of the last relation (i.e., hydraulic-electric connection) is demonstrated in this research.

In general, the electrical machines used in off-grid hydropower generation are today focused in three types: the squirrel-cage induction generator, the wound-rotor induction generator, and the permanent magnet (PM) synchronous generator [13]. However, it must be noticed that when considering our focus on SEIG for small-scale pico-hydropower (< 10kW) generators for rural and remote communities, factors as cost-effectiveness, simplicity, low operational and maintenance costs, and lifespan have equal significance as the efficiency and performance. Taking into account those factors and the power up to 10kW, the wound-rotor induction generator has to be discarded as a reliable option. Its rotor windings having a set of slip rings and brushes, or even considering the use of a power electronic converter that may not require slip rings, all this will result in a more expensive and less cost-effectiveness solution than considering a squirrel-cage rotor machine. For example, the rotor windings will be certainly subject to stresses during the generator's operation arising from its rotation and vibration, reducing the lifespan of the generator. The permanent magnet (PM) synchronous generator has, at first sight, three clear advantages relative to the SEIG machine: include self-excitation, thus not needing capacitors to supply reactive power, and has higher power density. However, not only cost is becoming today a major drawback due to the permanent magnets, but also it does not readily provide a constant voltage when its speed and the load current vary. Voltage regulation will thus demand a full power frequency inverter, reducing our necessary system's simplicity, low-cost solution and reliability, so critical in small-scale pico-hydropower systems to be spread in rural and isolated communities. Therefore, in this study, a squirrel-cage induction generator is considered.

Several studies have analyzed the performance of PAT systems for energy recovery in water systems. A PAT technology was tested with a laboratory prototype for a case study of an aqueduct in the city of Merano, Italy [14]-[15], in which the authors concluded to be possible to obtain 76% of the maximum efficiency of the turbine working in both reverse and direct mode. A pumping system of a micro-hydroelectric power plant in a rural farm in Brazil was designed with a turbine capable of performing both direct and inverse (PAT) modes coupled to a standalone isolated induction generator, considering a uniform rotational speed [16]. [12] started to analyze the global efficiency of the PATs in a laboratory prototype system. The tests were developed considering different rotor speeds and loads and determining the influence of the capacitor banks in the global efficiency of the machine. In experimental tests, the machine had to adapt to the different rotational speed in order to maximize the recovered energy when the flow was variable. In this first approach of a standalone sustainable solution when the PAT global efficiency was measured, the experimental result was 26% for the off-grid mode and about 62% for the on-grid mode. In this research, the developed models used to characterize the PAT system did not consider the variation of the electrical parameter of the generator.

This research contributes for a further study and optimization of off-grid PAT systems when they are installed in water distribution systems for both rural or remote areas. The most challenges arise in off-grid systems, in which the induction machine does not have an electrical grid to impose its electrical voltage and frequency as well as to supply its required reactive power. Typically, the excitation of the induction generators is done using a set of capacitor banks that impose its operating point [17]-[18]. This solution is called a self-excited induction generator (SEIG). The selection of capacitors must be done in the correct way so that the SEIG is sufficiently excited and that its operating point is the required one, *e.g.,* with the maximum output power [18]-[20]. The research focuses on the impact of the analytical model and its considerations to calculate the capacitor values that self-excite the induction generator (SEIG) and analyses its influence on the overall system operation point, mainly, regarding the overall efficiency and out of rated conditions.

The current research proposes a methodology to obtain the best efficiency of the PAT-SEIG system when operates under different speeds and loads. The use of this methodology will allow water managers who design the recovery systems to know the best rotational speed of the machine in order to maximize the energy recovered considering the resistive load circuit. This methodology was applied in a laboratory prototype, where the experimental (hydraulic and electrical) and numerical analysis were developed and compared, reaching interesting results and conclusions to improve the energy efficiency in the recovery water systems. The methodology is divided into three sections: section 1) is the introduction about the SEIG machines coupled to PAT systems; section 2) is subdivided into four subsections: simplified assumptions of neglecting the iron losses and the variations of electrical parameters identified, the analytical model is completed with the consideration of the iron losses, a methodology to include the variation of the electrical parameters and the induction machine is tested for different operation points to obtain the variation of the electrical parameters and where the turbine is tested to validate the developed finite element model; section 3) presents the comparison between analytical models, with and without the iron losses, and the impact of choosing the wrong capacitor values, in the influence of the variation of each induction generator electrical parameter in the capacitor value and in the final system efficiency. Finally, the main conclusions of the work are summarized in section 4.

2 Material and Methods

2.1 Problem identification and proposed solution

The values of the capacitances required to excite the SEIG were analyzed by [12] and these values were calculated for different resistive loads of electric circuit and different rotational speeds of the hydraulic machine. However, this interesting approach in the “off-grid recovery system” assumed not only that parameters of the equivalent electric circuit of the induction generator remained constant at its values obtained for the rated frequency and voltage values, but also the machine iron losses were neglected. Fig. 1 shows the previous results under these hypotheses. These results tended to overestimate the required capacitance (highest deviation of 18.8%) for speeds lower than its rated speed (910 rpm) and to underestimate (highest deviation of 23%) for speeds higher than its rated speed. These deviations are highly important because a wrong capacitance value may lead to one of the following problems: 1) non-excitation of the induction generator, or 2) its over-excitation leading to an overload of the machine. In Fig. 1, the continuous lines are the results for the numerical model simulation and the dashed lines show the analytical model [12].

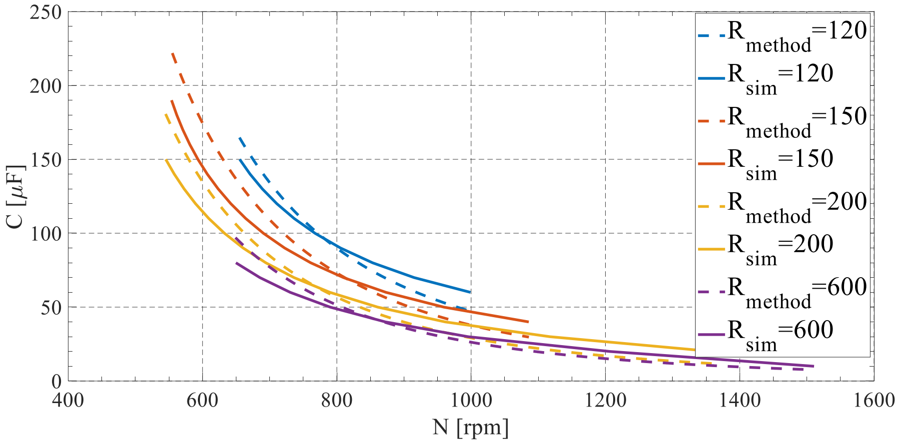

Fig. 1 – Capacitance per phase required for each induction generator rotor speed, for different resistive loads, and considering all electric circuit parameters fixed at its values obtained for the rated frequency and voltage SEIG values [12]. In continuous lines, the values obtained using the SEIG numerical model and in dashed lines the ones obtained using the old method [12].

When the capacitance value is over or underestimated for the induction generator operation, the problem is associated with the two hypotheses under which the equivalent circuit model was used by [12]: (i) the negligence of the iron losses representative parameter (R_m) and/or; (ii) the assumption of time-invariant parameters in the equivalent electric circuit of the induction generator, independent of its operating regime. Therefore, the study of the impact of both hypotheses in the values obtained for the capacitors is crucial in order to analyze the real behavior of this couple (PAT and SEIG) to reach the best efficiency in the recovery system. Considering this objective, a new analytical methodology for calculating the capacitors was developed. The equivalent circuit takes now into account the iron losses parameter (R_m), and new experimental no-load and rotor blocked tests were performed to verify which and how the equivalent circuit parameters of the induction machine change for different SEIG operating regimes.

2.2 Analytical methodology with R_m resistance (iron losses)

The analytical methodology follows the same steps that were presented by [12], but now including the iron losses in the induction generator equivalent circuit. Fig. 2 shows the per phase SEIG circuit. The scheme is divided into three parts: the inductive load (R_L, X_L), the capacitive reactance (X_c) and the equivalent electric circuit of the induction generator. In it, s is the machine slip, the R_s and R_r' parameters correspond to the stator resistance and the rotor resistance referred to the stator, respectively. X_s and X_r' correspond to the stator leakage reactance and the rotor leakage reactance referred to the stator, respectively. At last, R_m and X_m are parameters representative of the iron losses and the air-gap magnetic energy in the induction machine.

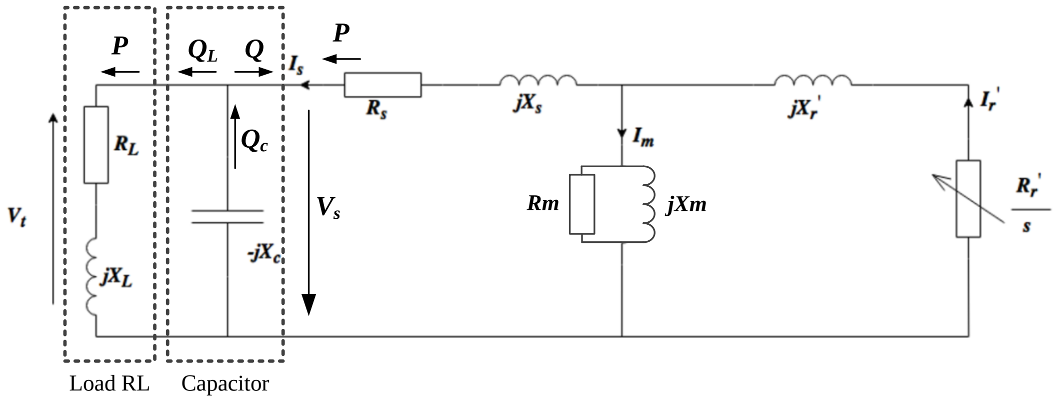

Fig. 2 – Equivalent electric circuit of the self-excited induction generator connected to an inductive load.

The equivalent electric circuit can be furthermore reduced to its per-unit values by dividing all parameters by the per-unit frequency, $a = \frac{f}{f_N}$ [21]. For an electrical quantity, the frequency can be expressed as $f = a \times f_N$ with all reactances given by eq. (1) to (5). When dividing these values by a, the resultant parameters are the reactance at the rated frequency, except for the capacitive reactance in (5).

$$X_s = 2\pi a f_N L_s \;\Rightarrow\; \frac{X_s}{a} = 2\pi f_N L_s = X_{s_N} \tag{1}$$

$$X_r' = 2\pi a f_N L_r \;\Rightarrow\; \frac{X_r'}{a} = 2\pi f_N L_r = X_{r_N} \tag{2}$$

$$X_m = 2\pi a f_N L_m \;\Rightarrow\; \frac{X_m}{a} = 2\pi f_N L_m = X_{m_N} \tag{3}$$

$$X_L = 2\pi a f_N L_L \;\Rightarrow\; \frac{X_L}{a} = 2\pi f_N L_L = X_{L_N} \tag{4}$$

$$X_c = \frac{1}{2\pi a f_N C} \;\Rightarrow\; \frac{X_c}{a} = \frac{1}{2\pi f_N C a^2} = \frac{X_{c_N}}{a^2} \tag{5}$$

Being the slip defined by the relative difference between the machine synchronous speed, N_s, and its actual mechanical speed, N, it can be rewritten in (6) as a function of the per-unit frequency a. Here, b is the per-unit speed, that is given by N/N_{s_N}.

$$s=\frac{N_s-N}{N_s}=1-\frac{N}{N_s}=1-\frac{N}{N_{s_N}a}=1-\frac{b}{a} \tag{6}$$

The remaining parameters (resistances) will be divided by a. As result, the electrical equivalent circuit can be redrawn as in Fig. 3.

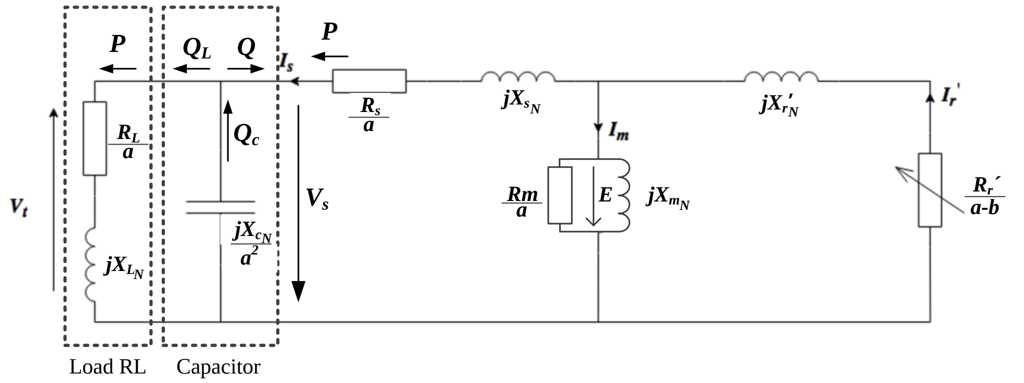

Fig. 3 – Equivalent electric circuit of the self-excited induction generator connected to the load based on the per-unit frequency a.

In order to assure the self-excitation of the induction generator, the total admittance (or impedance) of the equivalent circuit must be zero. In this research, the authors choose to use the admittance to facilitate the comparison between the new solution and the one obtained in previous studies without the R_m resistance [12], [21]. The admittances for the stator, Y_s, rotor, Y_r, and magnetization branch, Y_m, are given in (7). Those for the electrical load and capacitance are given by Eq. (8) and (9), respectively. The total equivalent circuit admittance can be determined using the parallel and series association, as given by Eq. (10). The values of capacitance and electrical frequency that lead to the null admittance can be calculated by setting the real and imaginary part of the total admittance to zero, Eq. (11) and eq. (12).

$$Y_s=\frac{1}{\frac{R_s}{a}+jX_{s_N}}\,,\; Y_r=\frac{1}{\frac{R_r'}{a-b}+jX'_{r_N}}\,,\; Y_m=\frac{a}{R_m}+\frac{1}{jX_{m_N}} \tag{7}$$

$$Y_L=\frac{1}{\frac{R_L}{a}+jX_{L_N}} \tag{8}$$

$$Y_c=-\frac{a^2}{jX_{c_N}} \tag{9}$$

$$Y_t=Y_L+Y_c+\left(\frac{Y_s(Y_m+Y_r)}{Y_s+(Y_m+Y_r)}\right) \tag{10}$$

$$\mathrm{Re}\{Y_t\}=0 \tag{11}$$

$$\mathrm{Im}\{Y_t\}=0 \tag{12}$$

The real part of the admittance, eq. (11), does not depend on the capacitance value. Therefore, the possible values of the per-unit frequencies that lead to the self-excitation of the induction generator can be calculated. Next, knowing the values of the per-unit frequencies and using the imaginary part of the admittance, eq. (12), the capacitance value can be computed.

From the decomposition of Eq. (11), the real part of the admittance is zero when the numerator expression shown in Eq. (13) is zero. The same can be done for eq. (12) and using the values the per-unit frequency from Eq. (13), the values of capacitance that assures the solution of Eq. (12) are given by Eq. (14) and (15). In annex are presented the expressions for each coefficient D_i, B_i, and A_i. Notice that including iron losses in the model through the R_m resistance, a solution of Eq. (11) had the degree of its polynomial equation Eq. (13) increased from five to six [12]. The solution of Eq. (13) will result in six possible per-unit frequencies, a_k, in which the machine will be self-excited. Being a per-unit frequency, only the real solutions correspond to possible steady-state ones. Therefore, Eq. (14) must be computed only for the solutions of a_k that are purely real. After calculating the possible values of capacitances C_k using (15), the minimum one will correspond to the minimum capacitance value that can excite the induction generator.

$$D_6 a^6 + D_5 a^5 + D_4 a^4 + D_3 a^3 + D_2 a^2 + D_1 a^1 + D_0 = 0 \tag{13}$$

$$X_{C_N} = \frac{A_8 a^8 + A_7 a^7 + A_6 a^6 + A_5 a^5 + A_4 a^4 + A_3 a^3 + A_2 a^2 + A_1 a^1 + A_0}{B_6 a^6 + B_5 a^5 + B_4 a^4 + B_3 a^3 + B_2 a^2 + B_1 a^1 + B_0} \tag{14}$$

$$C_k = \frac{1}{2\pi f_N a_k X_{C_{N_k}}}, \quad k = 1,..,8 \tag{15}$$

This method is not a linear process because the parameters of the induction generator will change for different operating points. Therefore, it is important to develop an advanced version of the previous analytical methodology, now capable of including the change of machine parameters according to its operating point and thus the respective capacitor values.

2.3 Analytical methodology considering variable equivalent circuit parameters

The calculation of the required capacitances for the excitation of the induction generator is now an iterative process due to the variation of the equivalent circuit parameters according to the machine operating point. To compute the induction machine electrical parameters, the voltage and electrical frequency of the machine that depends on the electrical parameters must be known. Additionally, the air-gap magnetic flux density ($\psi = \frac{E}{2\pi f}$, where E is the magnetization voltage, Fig. 3, and f is the electrical frequency) is an important factor to compute due to its influence on some induction machine parameters.

To facilitate the understanding of the novel analytical methodology, a flowchart of the developed algorithm is shown in Fig. 4. Initially, the electrical reactance is defined at the rated frequency of the induction generator. The induction machine used in this experiment had a rated frequency of 50Hz, therefore, all reactances are defined as $X_i = 2\pi 50 L_i$, such as $X_m = 2\pi 50 L_m$.

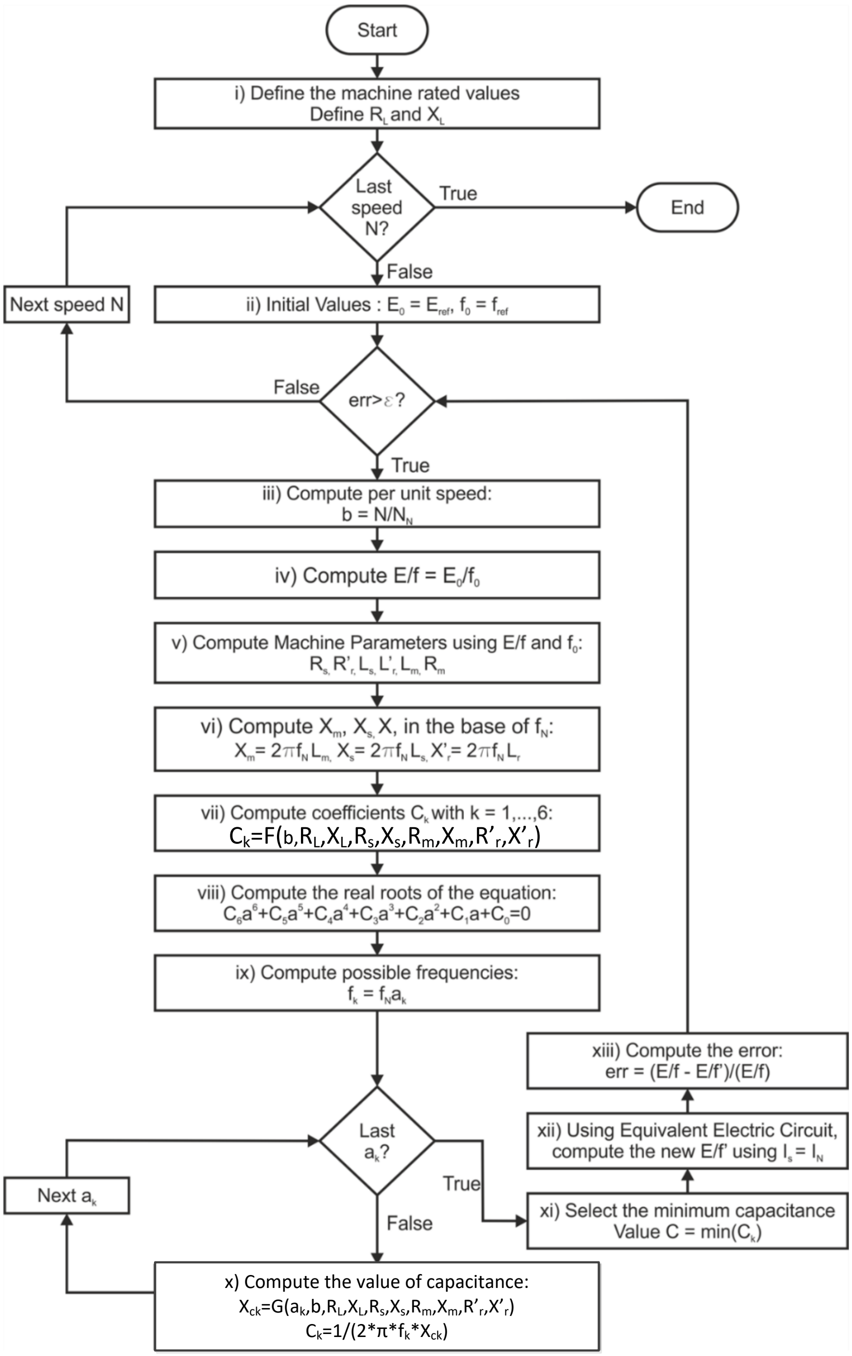

Fig. 4 – Flowchart describing the novel analytical methodology for the equivalent circuit parameters and associated capacitance values.

The algorithm starts in step (i) where the load electrical parameters (i.e., R_L and X_L) are defined. After this step, for each probable induction generator speed N, a series of two loops begin where steps (ii) to (ix) are repeated until the method converges for that speed value N. The first loop begins in step (ii) assuming an initial operating condition defined by a reference magnetization voltage, E_{ref}, and a reference electrical frequency, f_{ref}. This step establishes the initial magnetization level of the generator by its air-gap flux ψ, where E/f is an "image" of it.

Following, steps (iii) to (ix) can be computed. In steps (iii) and (iv) the per unit speed, b, and the E/f ratio are first defined. The per unit speed is computed by dividing the given machine speed, N, by its rated value, N_N. When the E/f ratio and the electrical frequency f_0 are defined, the generator parameters can be computed using the electrical machine parameters that were experimentally obtained a priori for different operating regimes of the generator, as described in detail in section 2.4 (step (v)). Follow, the reactance values are determined using the rated frequency of 50Hz (step (vi)).

Once the machine electrical parameters are known, the algorithm goes to steps (vii) and (viii) where the real roots of Eq. (13) are determined. In step (ix), within the previously computed solutions for a_k only the real ones are valid solutions. Selected the real parameters a_k, the possible electrical frequencies that lead to the self-excitation of the induction generator are computed by $f_k = f_N\ a_k$ in step (ix). For each possible frequency, the reactance and capacitance values required to self-excite the induction generator can be computed with Eq. (14) and (15), in step (x). After the calculation of all possible capacitance values, C_k, the minimum one must be chosen, (xi).

When the minimum capacitance value to self-excite the induction generator is known, the steady-state magnetization voltage E must be recalculated and compared with the one E_0 initially assumed in the step (ii). This can be done using the equivalent electric circuit of the self-excited induction generator connected to the load, as described in Fig. 3, and now solved in step (xii). When computing the equivalent electric circuit, it is required to define the stator phase voltage or stator current in the circuit. In this experiment, the authors choose to set the machine stator current to its rated value~~,~~ to maximize the generator electrical output power, $I_s=I_N$. Finally, if the error between the assumed E/f and the new E/f' value is still higher than a deviation ε, the steps (iii) to (xiii) must be repeated with the new E/f' value, until the method converges.

2.4 Changes in the equivalent circuit parameters of the induction generator

Fig. 5 shows the “wye” connected squirrel-cage induction machine used as SEIG. Its rated values are shown in Table 1. The machine has a rated efficiency of $\eta_N = 68\%$ and a nominal slip of $s_N = 9\%$. Using this machine, a set of new experiments were made to obtain the equivalent circuit parameters of the induction machine, not only for its rated condition, but now for different speeds and levels of magnetization (E/f), which in general occur in PATs with off-grid SEIGs. The question to be answered now is: which and how the generator parameters change considerably in order that new capacitance values will be desirable?

Fig. 5 – Induction machine used for experimental tests.

Table 1 – Nameplate data of the induction machine.

Frequency	50Hz
Voltage	400V
Current	1.6A
Output Power	0.55kW
Power factor	0.73
Speed	910rpm

2.4.1 No-load and Blocked Rotor Experimental Tests

Since the SEIG operating points vary in frequency and voltage, a set of experimental tests varying the voltage and frequency of the machine stator input were made to obtain its equivalent electric circuit parameters. Fig. 6(a) shows a diagram of the experimental set-up. In this set-up, the induction machine was powered by an isolated salient-pole synchronous generator driven by a DC motor. Using this approach, the DC motor speed will set the electric frequency and the synchronous generator excitation will set the induction motor voltage applied to the induction machine. Fig. 6 (a) also presents a photo of the experimental set-up showing the group DC motor/synchronous generator used. With this set-up, blocked rotor and no-load tests were accomplished in the induction machine (Fig. 6(b) by imposing a three-phase, balanced, and symmetrical stator voltages having different amplitudes and frequencies. These tests were done for frequencies that varied between 20 Hz to 60 Hz, in steps of 10 Hz. For each frequency, different voltage values were applied to the induction machine, but never exceeding more than 20% of its nominal current. The range of the selected frequencies was defined based on SEIG operation on previous work [12].

For each test, the phase r.m.s voltage and the current values, and also each phase active and reactive power consumed by the induction machine were measured. The electrical frequency and rotor speed were also acquired. The values showed that all phases of the induction machine were balanced, thus the description of the machine considering only an equivalent single-phase and the average values of each phase induction machine's parameters is possible.

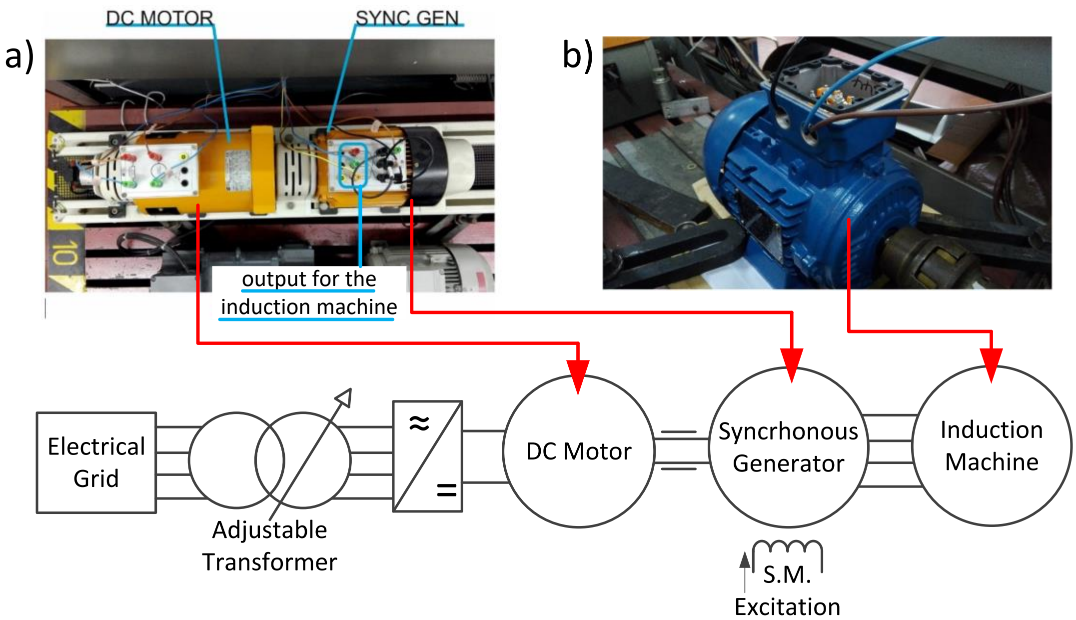

Fig. 6 – Experimental set-up: a) DC motor coupled to the salient-pole synchronous generator and the experimental diagram of the set-up, b) the induction machine feed.

The machine parameters were estimated using the data from all blocked rotor and no-load tests. The results are shown in Fig. 7. Each parameter is presented as a function of the magnetization level of the machine, *E/f*. During the experimental tests, the stator electric resistance was directly measured at the stator terminals, before and after the essays. It was verified that its value remained almost constant along all essays even for different stator current densities (R_s≈18.8Ω).

Fig. 7. (a) shows the sum of the stator and rotor leakage inductances ($L_s + L_r'$). These achieved values between 0.10H and 0.13H, remained almost independent of the magnetization level *E/f* of the generator, but had a slightly increase for electrical frequencies lower than the nominal value. Therefore, it was considered that stator and rotor leakage inductances remained constant for all levels of magnetization assuming an average value of about 0.11H.

Concerning the rotor resistance parameter R_r', it is necessary to remember that this is not the real value of the rotor resistance associated with the squirrel-cage conductors. It represents the Joule losses in the rotor conductors. Since it was obtained from the blocked-rotor essay, the slip is 1 and thus the electromotive force E that is induced in the rotor becomes given by $E = [R_r' + (j2\pi f L_r')]I_r'$. Dividing all terms by the electric frequency f, one obtains eq. (16) representing the partition of the magnetization flux $\phi_m \approx E/f$ in two parts: the useful one linking the stator and rotor, $\phi_{r\_useful} \approx (R'_r/f)I'_r$; and the leakage flux part not used in the electromechanical conversion process, $\phi_{r\_leakage} \approx j(2\pi L'_r)I'_r$.

Remembering that L'_r remains almost constant, it becomes important to understand how R'_r/f changes for different magnetization levels. Its values are plotted in Fig. 7. (b) for different frequency values varying from 20Hz to 60Hz. To help in to understand the behavior of it, three lines were added to the figure marking the points with the same current (I'_r =1.0, 0.75 and 0.5pu). Using Eq. (17) for each constant I'_r value, an increase of the magnetization flux *E/f* means that the R'_r/f ratio also increases proportionally because the rotor magnetic flux leakage represented by L'_r remains approximately constant (as seen previously in Fig. 7a). In Fig. 7b, this effect can be noticed when moving along each line of constant current. For the same current, the ratio R'_r/f increases with the increase of the magnetization level E/f.

$$\underbrace{\frac{E}{f}}_{\phi_m}=\underbrace{\frac{R'_r}{f}I'_r}_{\phi_{r\_useful}}+\underbrace{j(2\pi L'_r)I'_r}_{\phi_{r\_leakage}} \iff \phi_m=\phi_{r\_useful}+\phi_{r\_leakage} \tag{16}$$

$$\frac{E}{f}=\frac{R'_r}{f}\underbrace{I'_r}_{\approx\text{constant}}+\underbrace{j(2\pi L'_r)}_{\approx\text{constant}}\underbrace{I'_r}_{\approx\text{constant}} \tag{17}$$

Once, let's understand how R'_r/f changes for different magnetization levels. For the same frequency f, increasing E/f ratio is possible to increase the rotor current, I'_r. In this case, the R'_r/f ratio remains almost constant as described by eq.(18). This effect is verified in Fig. 7b, where, for the same frequency, the R'_r/f ratio remains almost constant for all magnetization levels.

$$\frac{E}{f}=\underbrace{\frac{R'_r}{f}}_{\approx\text{constant}}I'_r+\underbrace{j(2\pi L'_r)}_{\approx\text{constant}}I'_r \tag{18}$$

Analyzing Fig. 7c, the magnetizing inductance, L_m, is a function of the magnetization level, E/f, showing similar values for the *whole* set of tested electric frequencies. Using the nameplate data of the generator in Table 1, the nominal level of magnetization per phase is $230/50 = 4.6$ V Hz^{-1}. This value of magnetization level is usually taken into account in the design of an electrical machine, corresponding to the knee point of the B-H curve of the ferromagnetic material core. This is in agreement with the results presented in Fig. 7c for 50Hz since, for lower levels of magnetization E/f, the magnetic core is in its linear zone and L_m stays nearly constant. When there are lower L_m values and the magnetization level is near the nominal value, the L_m parameter tends to decrease.

At last, Fig. 7d shows the evolution of the magnetization resistance R_m divided by the electrical frequency, f, as a function of the magnetization level, E/f. Independent of the electric frequency, R_m increases as the magnetizing flux in the generator increases. The power losses in the magnetization resistance are associated with the iron losses due to the eddy current and the hysteresis effects. In typical magnetic materials, both hysteresis and eddy current power losses depend on the magnetic flux density in the iron core, B, as shown in eq. (19). However, the hysteresis losses are also proportional to the electric frequency, f, while eddy current losses are proportional to the square of the frequency, f^2.

$$P_m=k_hBf+k_eBf^2 \tag{19}$$

Using the induction machine electric circuit in Fig. 3, the relation between the magnetization power, P_m, and the ratio R_m/f is given by (20).

$$P_m=\frac{E^2}{R_m}=\frac{E^2}{f}\frac{f}{R_m} \tag{20}$$

Knowing the magnetic flux density is a linear "image" of E/f until the knee point of the B-H curve (E/f=4.6V/Hz), and using Eq. (19) and (20), the ratio R_m/f can be easily connected to the E/f as shown in eq. (21). This relation is evident since the eddy current losses are usually neglected compared with the hysteresis ones, as in (22). Therefore, increasing the magnetization level E/f, the R_m/f ratio increases (Fig. 7d), increasing the magnetization power losses too.

$$P_m = \frac{E^2}{f}\frac{f}{R_m} = k_h\left(\frac{E}{f}\right)f + k_e\left(\frac{E}{f}\right)f^2 \Leftrightarrow$$
$$\Leftrightarrow E\frac{f}{R_m} = k_h f + k_e f^2 \Leftrightarrow \frac{R_m}{f} = \frac{E}{k_h f + k_e f^2} \tag{21}$$

$$\frac{R_m}{f} = \frac{E}{k_h f + k_e f^2} \xrightarrow[k_h f >> k_e f^2]{} \approx \frac{E}{k_h f} \tag{22}$$

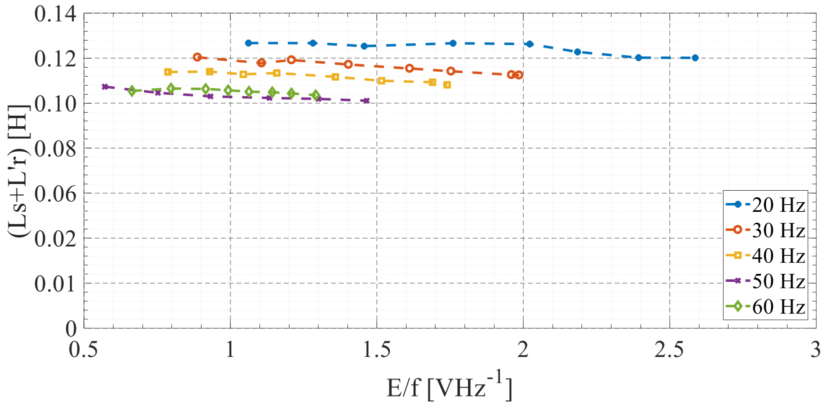

a)

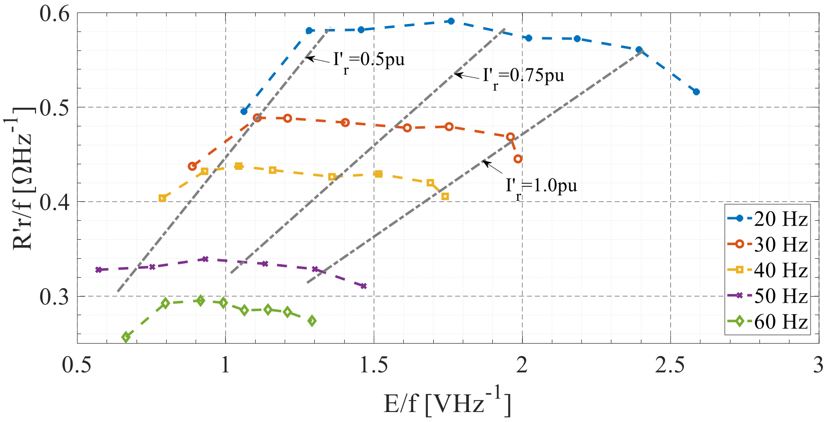

b)

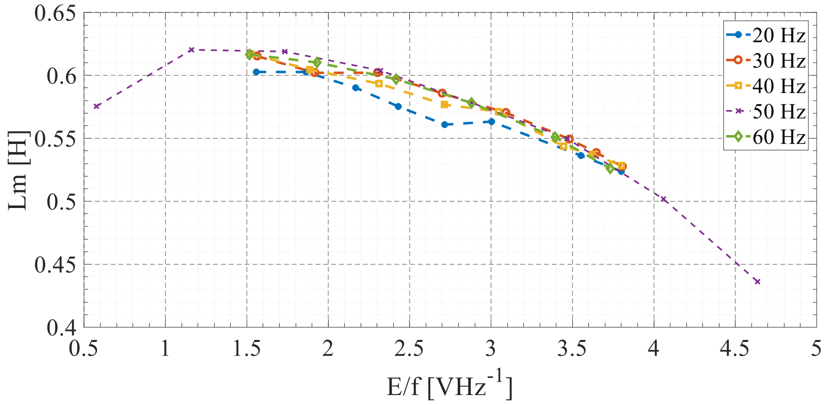

c)

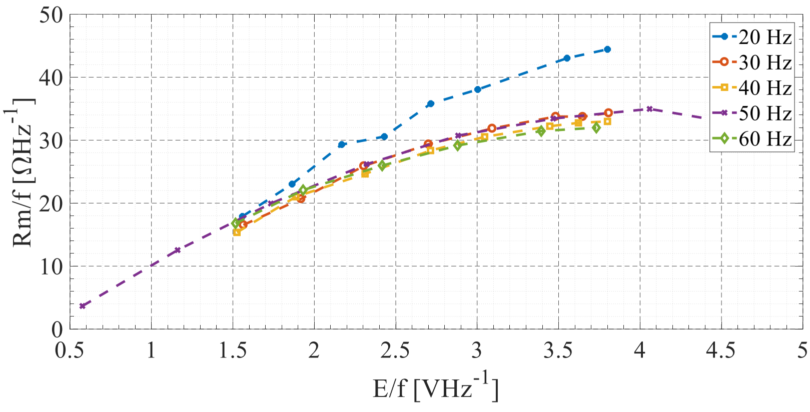

d)

Fig. 7 – Experimental results for each electrical parameter, a) L_s+L'_r, b) R'_r, c) L_m and d) R_m, depending on the *E/f* ratio.

In summary, the answers for the previous question on "…which and how the equivalent circuit parameters of the induction machine change for different SEIG operating regimes?..." are:

1) Increasing the generator's magnetization level *E/f*, L_m decreases, ratio R_m/f increases and ratio R'_r/f remains almost constant. Hence, not only the parameter L_m must be considered in the equivalent circuit, but also R_m and R'_r must have its value "tuned" to the generator's operating point;
2) At last, parameters L_s and L'_r can be assumed constant, independent of the generator's operating point.

2.5 Experimental tests of the SEIG

The experimental set-up used to determine the values of the capacitors required to self-excite the SEIG is shown in Fig. 8. In this set-up, the SEIG was mechanically coupled to a DC motor which simulated the load imposed by the shaft of the PAT, thus setting the speed and mechanical power of the SEIG (Fig. 8.a). The SEIG is electrically connected to the capacitor and the resistor bank in parallel (Fig. 8.b). A Fluke power logger was connected to the stator of the SEIG to measure each phase voltage, current, active and reactive power, and also a multimeter was connected to the SEIG to measure its electrical frequency.

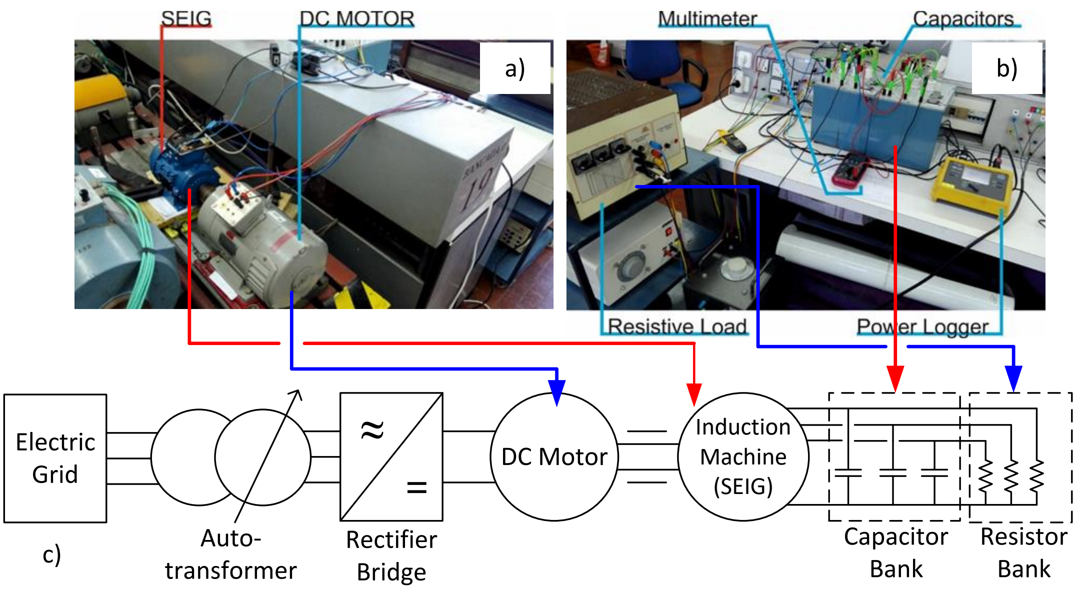

Fig. 8 – Experimental set-up for the determination of the capacitance values for self-excitation of the SEIG. a) SEIG and DC motor, b) Capacitor bank, resistive load, power logger and auxiliary measurement equipment, and c) the electrical diagram of the experimental set-up.

The following procedure was applied to each electrical load value to determine the points of self-excitation:

1. A capacitance value is chosen, and the speed is increased until the SEIG starts to the self-excite. This value of the SEIG speed is named ω_{start}.

2. After the self-excitation, the generator speed is increased until the maximum stator current is reached. These values correspond to the SEIG speed that leads to the rated current of the chosen value of capacitance.
3. Then, the speed is dropped until the SEIG can no longer be self-excited. This is the minimum speed for which the generator can still be excited, ω_{min}.

The results of these experiments are shown and analyzed in Section 3.

2.6 Hydraulic experimental tests

An experimental set-up of the overall PAT-SEIG system was developed and used in [12], which is in CERIS-Hydraulic Lab of Institutor Superior Técnico, University of Lisbon. The experimental set-up consists in a closed loop water system with a radial PAT turbine connected to a SEIG machine (I), a recirculating pump (II), an air vessel (III) and a flow control tank (IV), as shown in Fig. 9a. The experimental set-up is shown in Fig. 9b, where each element is identified: (1) hydraulic PAT machine; (2) induction generator; (3) air vessel; (4) pressure transducer; (5) wattmeter to register each current phase, voltage and power; (6) resistive loads; (7) capacitor banks; and (8) switch to connect and disconnect the capacitors. During the experimental tests, an electromagnetic flowmeter was used to register the discharge flow rate, transducers connected to a picoscope to measure the pressure and a frequency meter to register the turbine speed.

A)

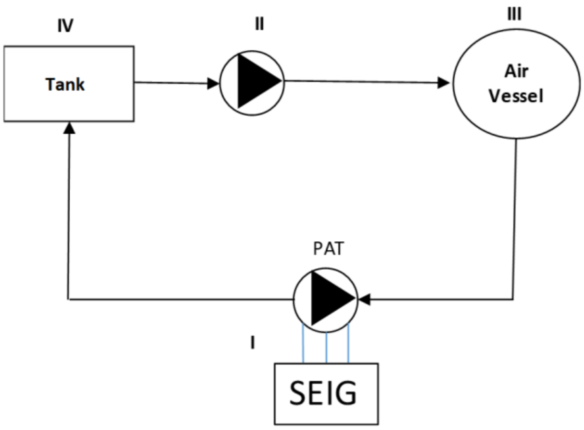

B)

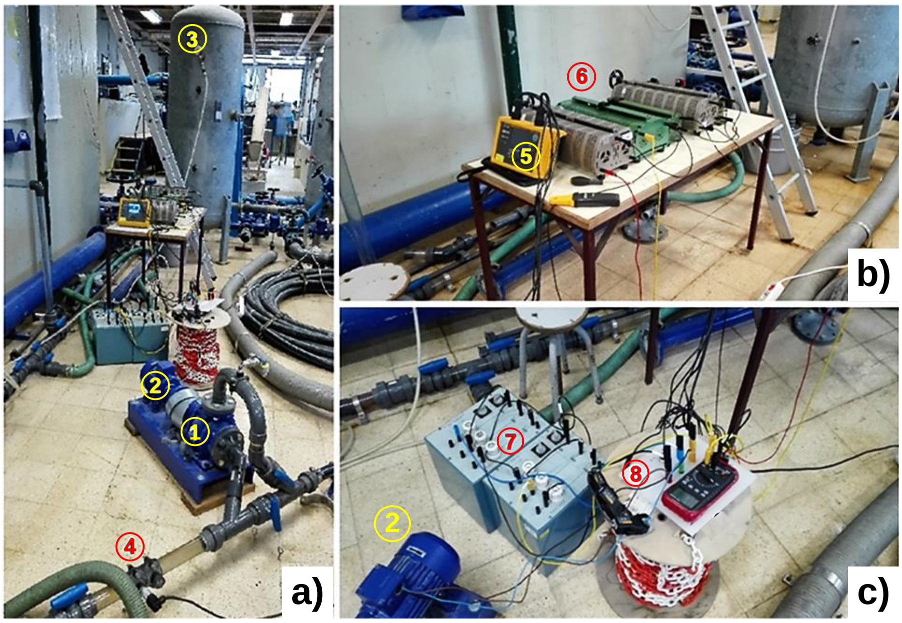

Fig. 9 – Hydraulic experimental set-up: A) Scheme of the hydraulic system. B) Experimental set-up: (a) overall PAT view, (b) loads and measurements and (c) SEIG system.

The electrical experimental tests were replicated now in the hydraulic system, where a PAT hydraulic machine drives the SEIG feeding the electrical loads. With these tests, PAT-SEIG system efficiency curves were obtained. Hence, the overall system efficiency, η_{overal} in eq. (23), can be estimated by dividing the electrical load active power, P_{load}, by the turbine hydraulic power, P_{hyd}.

$$\eta_{overall} = \frac{P_{load}}{P_{hyd}} \tag{23}$$

For each electrical load, the SEIG, PAT and overall PAT-SEIG system efficiencies were computed using Eqs. (24) to (25), respectively,

$$\eta_{SEIG} = \frac{P_{load}}{P_{mech}} \tag{24}$$

$$\eta_{PAT} = \frac{P_{mech}}{P_{hyd}} \tag{25}$$

$$\eta_{overall} = \eta_{PAT}\eta_{SEIG} \tag{26}$$

where the η_{SEIG}, η_{PAT} and $\eta_{overall}$ are the SEIG, the PAT and the overall system efficiencies, respectively. Terms P_{load}, P_{mech} and P_{hydr} are the electrical load power, mechanical power, and hydraulic power, respectively.

3 Results and Discussion

After the description of the used equivalent circuit models of the induction machine for the capacitance calculation, as well as the methodology to calculate the equivalent circuit parameters, the PAT-SEIG results are now presented and discussed. In this section, the following aspects are focused:

1. Results comparison between the methodology with and without considering the iron losses parameter, R_m:

   Considering all machine parameters fixed, the analytical results provided by the equivalent circuit without the R_m resistance [12] are compared with the ones obtained with R_m (equivalent circuit presented in section 2.4). Without considering the variation of the remaining circuit parameters, the error between the experimental results and the analytical ones was high, mainly for low machine speeds. This could lead to an over-estimation of capacitance value required to self-excite the induction generator and to non-normal operating regimes, higher than its rated conditions. These non-normal conditions may overheat the generator and reduce its lifetime or cause permanent damage;

2. The influence of the variation of each equivalent circuit parameter in the capacitance value calculation:

   With only one parameter changing and keeping the others fixed, the analytical results using the equivalent circuit are compared with the experimental ones. This analysis helps to understand the influence of each parameter in the capacitance value calculation and then decide the most relevant ones;

   The SEIG electrical circuit parameters considered in the selection of the capacitance were:

   - Variable L_s=L_r' (stator/rotor magnetic leakage);
   - Variable R_r' (Joule losses in the rotor electric conductors);
   - Variable R_m (iron Joule losses), and;
   - Variable L_m (magnetic energy in the air-gap).

3. The electrical, hydraulic and global efficiency of the *PAT-SEIG* system:

   The global efficiency is compared with the one obtained in [12], where the machine's equivalent circuit parameters were considered always constant.

3.1 Generator’s equivalent circuit models and the impact of the wrong capacitance value

The magnetization resistance (R_m) introduces a higher complexity in the analytical solution using the equivalent circuit of the induction generator, increasing the order of the polynomial solution from a fourth to sixth order, as Eq. (13) shows. Using the experimental set-up described in section 0, the self-excited induction generator was tested *off-grid* at different speeds and loads. Fig. 10 shows the results considering the induction machine parameters fixed at the values obtained for its rated frequency and voltage, for both circuit models ($R_m = \infty$ and $R_m \neq \infty$), and also the experimental results obtained for the induction generator operating at its rated current. When all parameters were fixed, there was no significant difference between the models’ results (less than 1% of the root mean square error (RMSE)). However, the error between the experimental and model’s results were about 51% (RSME), being higher for lower speeds. This could lead to an overload state (i.e., stator current higher than its rated value) and reduce the lifetime of the induction generator. To study the impact of choosing the wrong capacitance value for the SEIG operation, the stator current was computed for the values of the capacitance given by the two models with the fixed parameters.

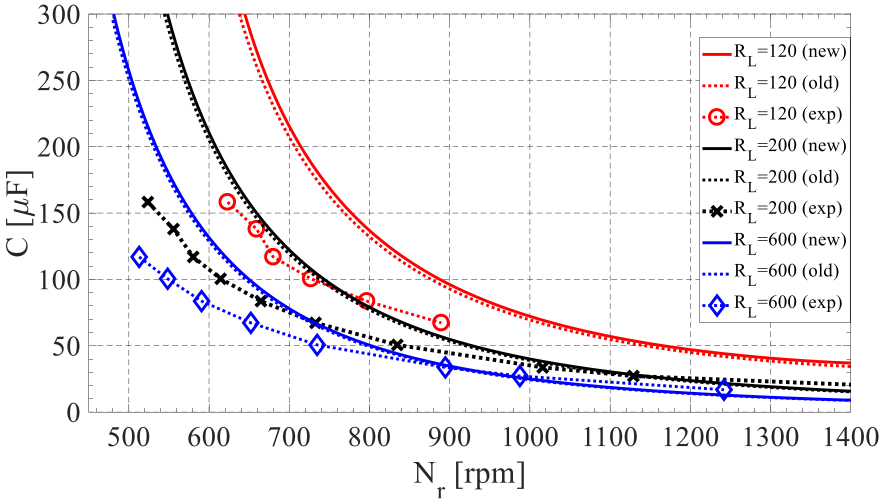

Fig. 10 – Capacitance required for each generator rotor speed, for different resistive loads, considering all parameters fixed. In continuous lines are the results for the analytical model considering R_m, in dot line for the analytical model without R_m [12] and in “o”, “x” and “◊” the experimental results.

Fig. 11 presents the steady-state results for the ratio between the SEIG stator current and its rated value for different speeds and loads. As it can be verified, the stator current could reach up to three times its rated value, which in a steady-state would imply a high increase of the machine’s temperature lead to a failure of its winding’s insulation. For higher speeds and lower loads (R_L=600Ω), the stator current decreases below the rated value, therefore decreasing the SEIG output electrical power.

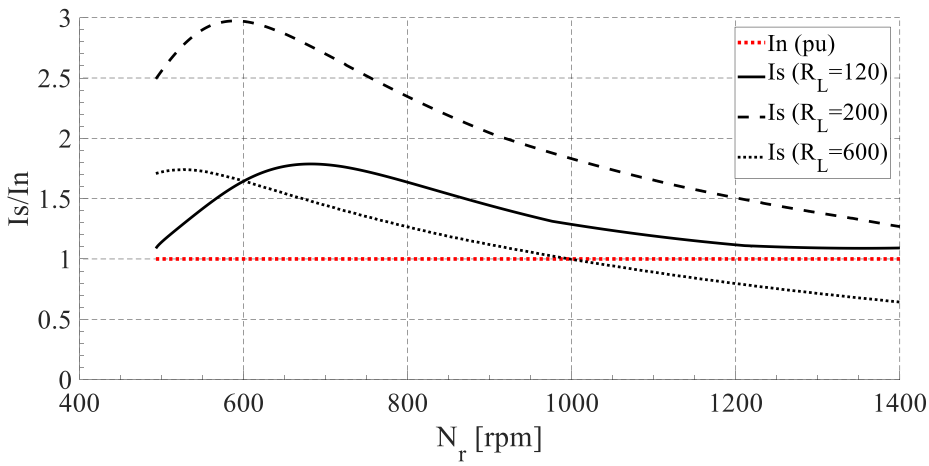

Fig. 11 – Influence of using wrong capacitance values in the induction machine stator current, for the different loads and rotational speeds.

All these results highlight the importance of choosing the right capacitance values to limit the current of the machine to its rated value and, at the same time, to be sufficient to guaranty the self-excitation of the induction generator.

3.2 Influence of the change in the generator's equivalent circuit parameters

As verified in section 2.4, the SEIG equivalent circuit parameters change with its voltage and electrical frequency, in consequence of its magnetization level. To create a methodology for the study of the influence of the parameters in the circuit, the following cases were analyzed, and the deviation was quantified between the experimental and the model's results using the root mean square error. Note that some previous studies already considered the equivalent electric circuit without iron Joule losses and with a variable L_m parameter [12] e [22] and other including the iron Joule losses, with a variable L_m and all other electrical circuit parameters being fixed [23]. Therefore, considering our methodology, a comparison between different equivalent electric circuits is analyzed.

1) Variable R_r' (Joule losses in the rotor electric conductors) and L_s=L_r'=0.055H, R_m=1000Ω, L_m=0.55H;
2) Variable L_s=L_r' (stator/rotor magnetic leakage) and R_r'=18Ω, R_m=1000Ω, L_m=0.55H;
3) Variable R_m (iron Joule losses) and L_s= L_r'=0.055H, R_r'=18Ω, L_m=0.55Ω;
4) Variable L_m (magnetic energy in the air-gap) and L_s= L_r'=0.055H, R_m=1000Ω, R_r'=18Ω, and [23];
5) All electrical circuit parameters changing with the generator's magnetization level.

All results are shown in Fig. 12a-d and can be summarized as follows:

1. Variable R_r': The circuit model used for comparison between results is the one that considers the iron Joule losses parameter, R_m. Fig. 12 shows the results for the capacitance values required to guaranty self-excitation of the SEIG at its rated current with different speeds and loads. In Fig. 12 a), the results showed for the two equivalent electric circuit models ("all fixed" and "var. R_r"), with all parameters fixed at its rated values (dotted lines) and with the rotor resistance, R_r', changing with frequency and stator voltage values (continuous lines) as previously achieved in Fig. 7. It is possible to verify in Fig. 12 a) that the new model results of "var. R_r" (continuous lines) were close to the experimental ones, but they still presented a high deviation for lower speeds (Maximum RMSE=40.35% for the R_L=120Ω).

2. Variable L_s=L_r': Fig. 12 b) shows the results for both equivalent electric circuit models ("all fixed" and "var. L_s") considering the stator and rotor magnetic leakage parameters changing (L_s= L_r'). The error between the experimental and the model results increased due to the increase of magnetic leakage inside of the SEIG. With the increase of magnetic leakage, the machine requires more reactive power and, therefore, the required capacitance value is higher. For low and medium loads, R_L=*600*Ω and R_L=*200*Ω respectively, this increase was not significant. However, for higher loads, R_L=*120*Ω, the capacitance values from the "var. L_s" model do not guaranty the self-excitation of the induction generator for speeds lower than 730rpm.

3. Variable R_m: When the inclusion of the variable magnetization resistance R_m was considered in the equivalent circuit "var. R_m", the results were almost the same as having a fixed ones (Fig. 12c)). This was expected because the difference of considering or not this resistance was already seen as insignificant.

4. Variable L_m: Fig. 12d) shows the results for the required capacitance values to excite the SEIG at its rated current, including a variable magnetization inductance coefficient "var. L_m". The results were shown for the model with all parameters fixed at its rated values (dot lines and "all fixed") as well as with the magnetization induction parameter, L_m, changing with frequency and voltage applied (continuous lines). Using a changing L_m parameter, the analytical results were much closer to the ones obtained experimentally. The error between results reduced from 51% to 17.9%.

5. Finally, Fig. 13 shows the results for both equivalent electric circuit models ("all fixed" and "all var"), with all the SEIG parameters changing according to the operating regime of the machine. For this situation, the maximum error was 13.2% between the experimental and model results. Table 2 compiles the errors between the analytical and experimental results for all studied scenarios.

Table 2 – RMSE between experimental and analytical results

Parameter	**R_L=120Ω**	**R_L=200Ω**	**R_L=600Ω**
All fixed [12]	50.8%	48.8%	42.7%
R_r’ variable	40.4%	39.9%	37.2%
R_m variable	49.9%	48.1%	42.1%
L_s, L_r’ variable	*	52.93%	42.4%
L_m variable [23]	11.2%	16.9%	17.9%
All variable	7.9%	11.0%	13.2%

* It was not possible to excite for with the range of available capacitor values.

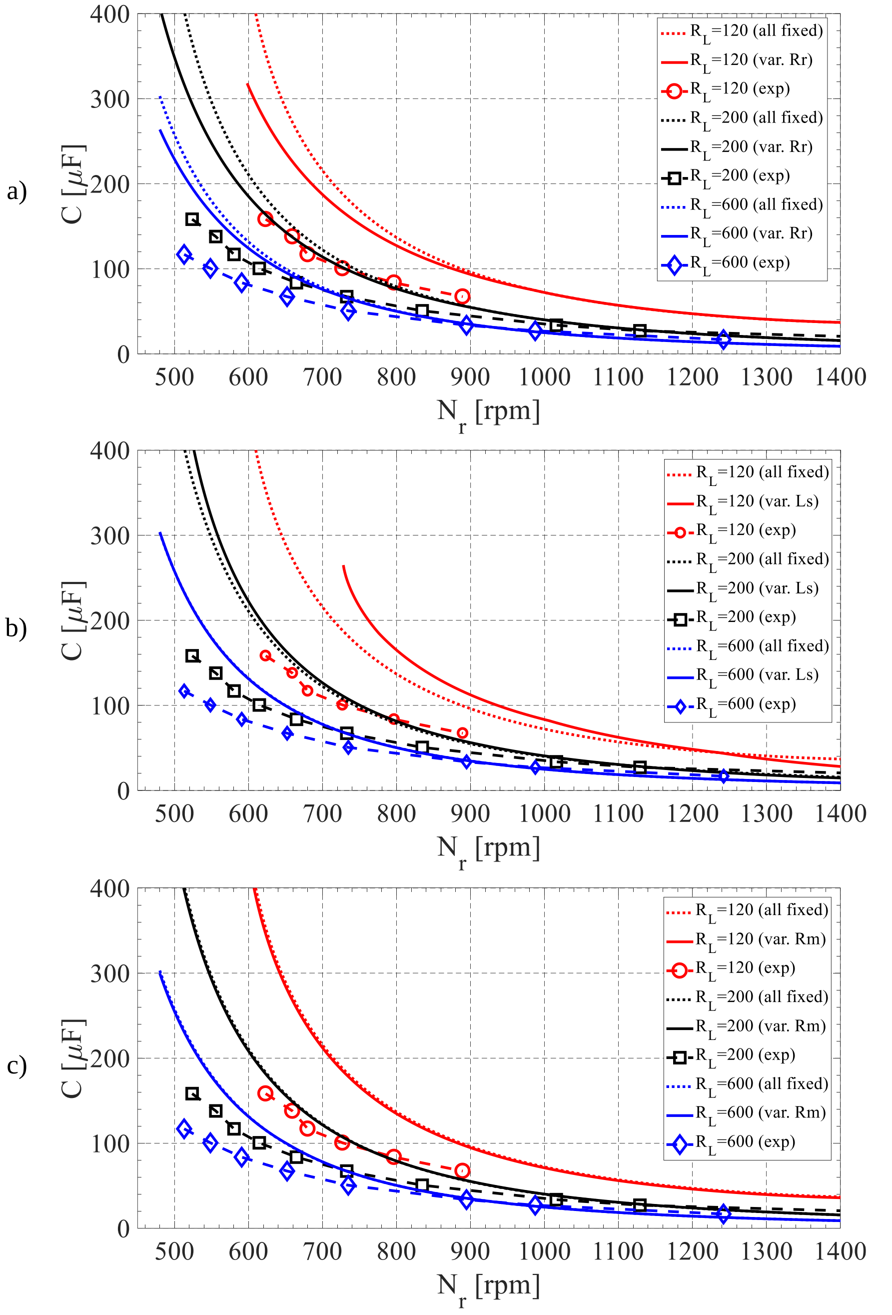

d)

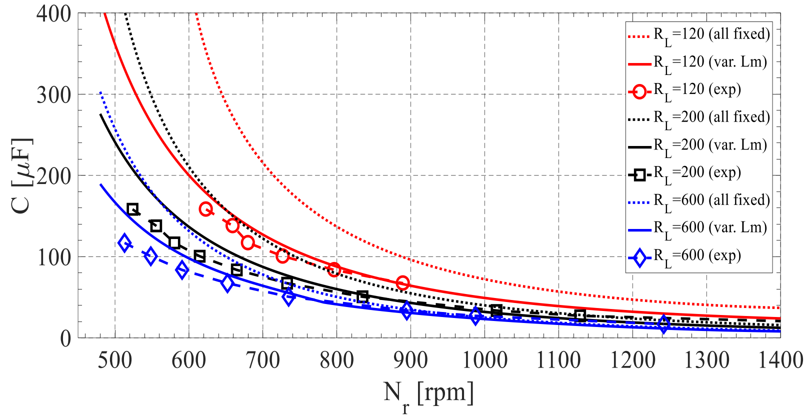

Fig. 12 - Capacitance required for each generator rotor speed and resistive loads obtained using the model with only one parameter changing: a) R_r' variable; b) L_s variable; c) R_m variable and d) L_m variable [23]. In dotted lines are the results for the analytical model (considering R_m) with all fixed parameters [12], in continuous lines for the analytical with R_r' changing and in "o", "x" and "◊" the experimental results.

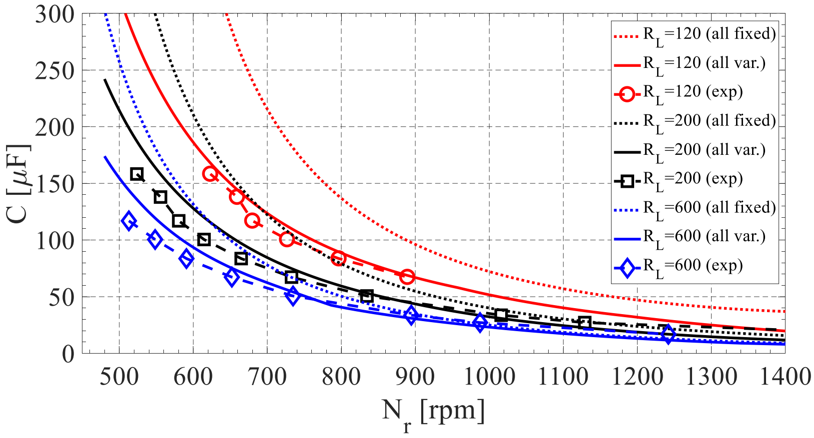

Fig. 13 - Capacitance required for each generator rotor speed and for different resistive loads, considering all parameters changing. In dotted lines are the results for the analytical model (considering R_m) with all fixed parameters [12], in continuous lines for the analytical with R_r' changing and in "o", "x" and "◊" the experimental results.

Table 2 clearly indicates that the magnetization inductance coefficient, L_m, has the highest influence on the accuracy of the model results. This parameter changes with the ratio *E/f*, where *E* is the magnetization voltage, and *f* is the electrical frequency. It changes with the magnetization level of the induction generator. Fig. 14 shows the evolution of the *E/f* ratio (Fig. 14a in red) and the evolution of the L_m (Fig. 14b in black) for each SEIG speed and load. Considering *E/f* an "image" of the magnetic flux inside the machine, for higher values (e.g. $R_L=600\Omega$ in Fig. 14a, in red dotted), the magnetic flux increased to points near the magnetic circuit saturation and, therefore, the L_m parameter decreased ($R_L=600\Omega$ in Fig. 14b, dotted lines). For lower values of *E/f* (e.g. $R_L=120\Omega$ in Fig. 14a, in red dotted), the magnetic flux remained almost constant inside the linear part of the *B-H* characteristic and, therefore, the L_m parameter presented small changes for higher speed values ($R_L=120\Omega$ in Fig. 14b, continuous lines).

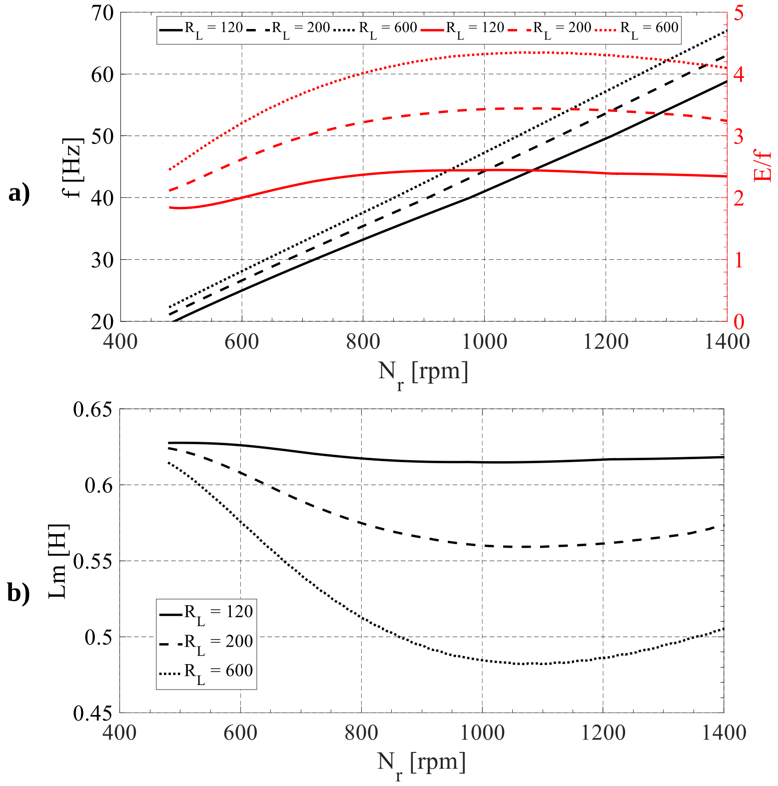

Fig. 14 – Evolution of SEIG parameters: a) the frequency and E/f characteristic and b) the corresponding L_m parameter for each rotor speed and resistive load, with all parameters changing.

3.3 SEIG/PAT/Overall efficiencies

The SEIG efficiency can be estimated using its analytical model, however, due to the turbine and hydraulic system complexity, a detailed model was required. To obtain an accurate PAT model, a CFD (computational fluid dynamics) model was developed and validated with experimental results [24]. The development of CFD model enabled to know the mechanical power in the PAT shaft for each rotational speed and, therefore, the possibility to identify the SEIG, PAT and global efficiencies for all range of rotational speeds that were obtained experimentally. Fig. 15 shows the CFD model used in the hydraulic simulation and Table 3 shows the mean square error between the simulated and experimental tests for different operation points.

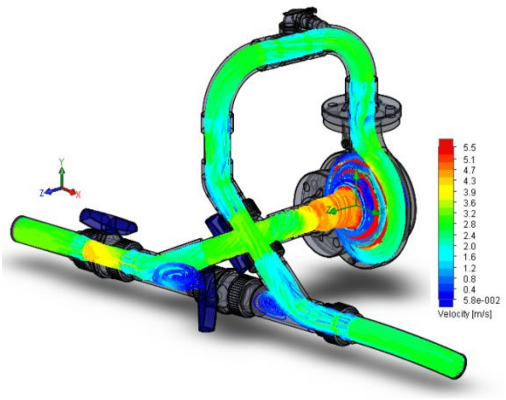

Fig. 15 – CFD model of the PAT.

Table 3 – Mean square error for each rotational speed.

N	**Mean Square Error (%)**	
	Head	**Efficiency**
785	1.97	2.62
908	2.66	2.41
1020	2.64	2.33
1145	2.36	3.05
1235	2.68	9.44
1460	8.69	9.66

Fig. 16 shows the SEIG, PAT and overall system efficiencies (eff) for the different rotational speeds and resistive loads, 120, 200, 300, 400 and 600 Ω. The SEIG system efficiency presents different behavior for different loads and rotational speeds, particularly, low-efficiency values for lower speeds and higher values for higher speeds. The maximum SEIG efficiency was reached from 1240 to 1450 rpm with 65% to 68.5%, with the resistive loads of 200 to 400Ω (see Fig. 16b-d). The maximum value for the global maximum efficiency was 40.0% for the rotational speed near 1450 rpm.

Our research clearly shows, for the first time, that the maximum PAT-SEIG overall efficiency is not the same independent of the rotational speed and torque, in other words, dependent of the PAT-SEIG operating point (i.e., flow and head). The analysis of the different resistive loads was similar. If a resistive load of 120Ω is considered, the maximum SEIG efficiency was 57.0% for a speed of 786 rpm and the maximum overall efficiency was 35.3%, when the speed was around 840 rpm. For a resistive load of 200Ω, the maximum SEIG efficiency was 65.5% for a speed of 1450 rpm and the maximum overall efficiency was 39.2%, when the speed is 1200 rpm. For a resistive load of 300Ω, the maximum SEIG efficiency was 68.4% for a speed of 1450 rpm and the maximum overall efficiency was 40.0%, when the speed is 1240 rpm. For a resistive load of 400Ω, the maximum SEIG efficiency was 68.4% for a speed of 1450 rpm and the maximum overall efficiency was 39.8%, when the speed is 1340 rpm. Finally, when a resistive load of 600Ω was considered, the maximum SEIG and overall efficiencies were 65.5% and 39.0% for the speed of 1450 rpm and 1410rpm, respectively.

When the overall PAT-SEIG efficiency is compared with recently published research [12], the overall system efficiency increased from 26% to 40%, showing an improvement of + 53%. This is clearly due to a more precise computation of the capacitance values. In our previous work [12], it was lower due to not been taken into account the change of the induction generator parameters for different levels of magnetization and rotational speed. However, it is important to emphasize that our previous study in [12] enabled to establish the base to develop this sensitivity research analysis about the significant behavior of the PAT+SEIG system.

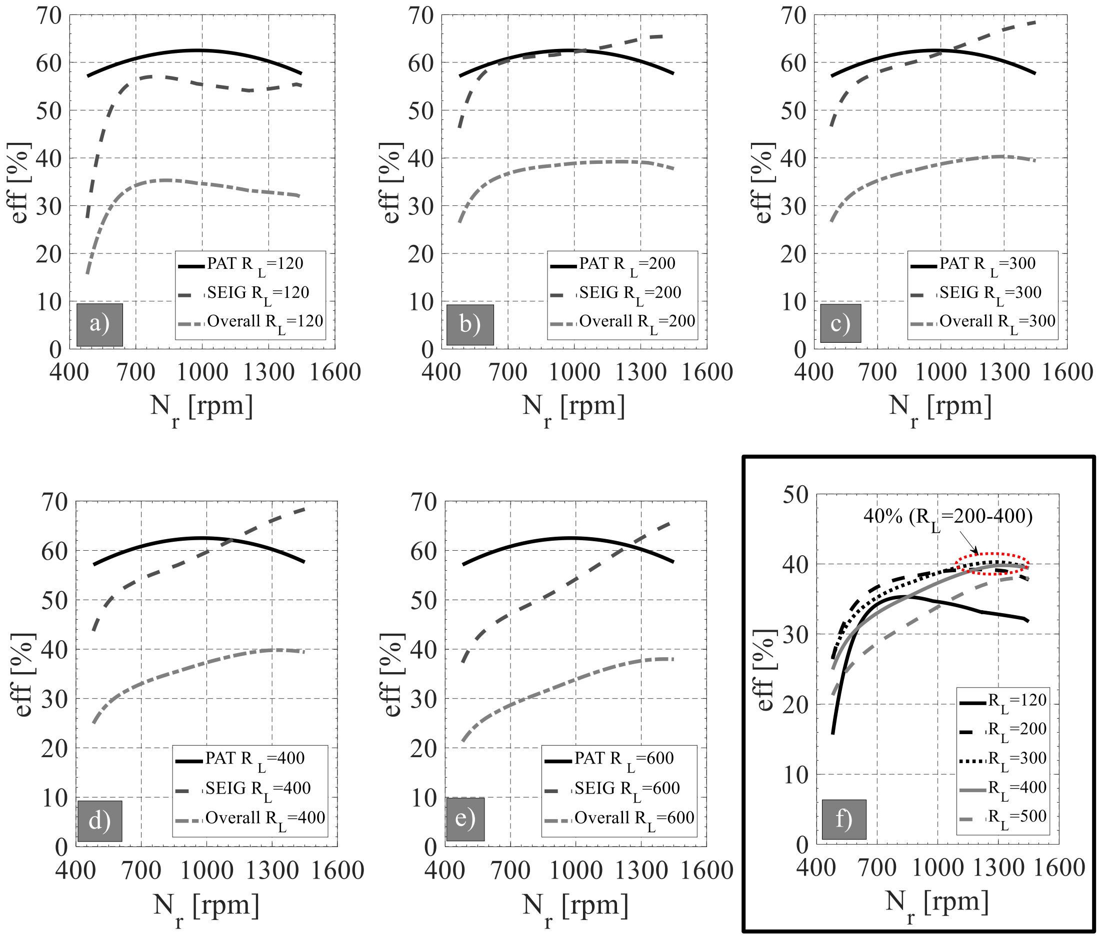

Fig. 16 – Evolution of the SEIG, PAT and overall system efficiencies for different rotor speeds and for the resistive load of R_L=[120 (a) 200 (b) 300 (c) 400 (d) 500 (e)] Ω. Comparison between overall efficiencies in (f).

In Fig. 17a and b, the active and reactive power flowing from the induction generator and its power factor are presented, respectively. Fig. 17a shows that for low-speed values, the reactive power required to excite the SEIG is much higher than the active power produced, while for higher speed values, the active power increases and the reactive power reduces. This was expected in SEIG, where its voltage was not defined by the electrical grid but was defined for the capacitor value and the impedance of the induction generator. Therefore, the reactive power required to excite the SEIG was much higher than when the machine was connected to the electrical grid. As result, for the rated speed of the induction generator, N_r=910 rpm, the active power, and power factor were lower than its rated values, 550W and 0.73, respectively. Only for high SEIG speeds the rated active power and power factor were reached (see Fig. 17b).

From Fig. 17a it is also possible to verify that the same generated power can be obtained for R_L=200Ω and 300Ω, with P=606W, however different reactive powers are required, Q=708 var for R_L =200Ω and 887 var for R_L =300Ω.

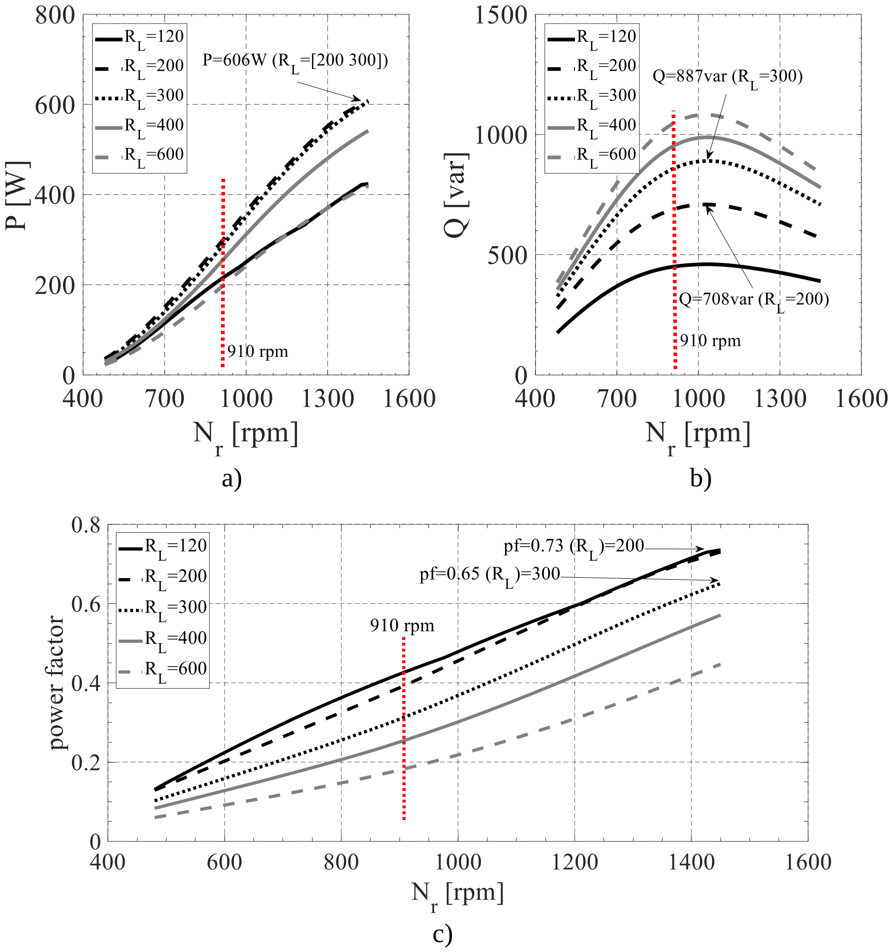

Fig. 17 – Active (a) and reactive power (b) and power factor (c) of the SEIG for different rotor speeds and for the resistive load of R_L=[120 200 300 400 600] Ω.

Figures 16 and 17 show the impact of the load and capacitance values in the PAT-SEIG efficiency. The development of this analysis is crucial to understand the symbiosis between electrical and hydraulic parameters when the water managers want to install recovery systems isolated to the grid, achieving the best overall efficiency that will depend on the PAT-SEIG operating condition, as shown in the paper.

4 Conclusions

The research establishes the influence of the capacitor values to SEIG on the overall system operation points, mainly, regarding the overall efficiency and non-normal conditions. From previous studies, the lack of accuracy of analytical models based on the equivalent electrical circuit of the SEIG was verified when considered fixed electrical parameters and neglecting the iron Joule losses. This analysis demonstrated that it is crucial to develop an accuracy energy models when the pump working as turbines are installed in water systems and they are "off-grid". The improvement of the PAT systems efficiency is crucial to improve the energy recovery in water distribution systems. Currently, the energy studies shows the recoverable energy is 10% of the used energy in the water distribution consumption although this recovery is not installed yet. The developments of this research are of utmost importance, showing that the SEIG parameters have a high influence on the energy recovery efficiency and that the choice of the capacitor values must consider its variance. These considerations must be considered in future researches, not only focusing the hydraulic machine.

The new analysis showed the model accuracy greatly increased when the variation of the SEIG electrical parameters was considered as a function of the electrical frequency and applied a voltage when the iron Joule losses, Rm, were considered in the model. To analyze it, a deep campaign of electrical and hydraulic tests was developed in order to compare and measure the error with the analytical model. From experimental tests, it was verified R_r, R_m, and L_m had a high oscillation for different speeds and loads. Both R_m and L_m parameters mainly depend on the magnetic flux (E/f (magnetization voltage/electrical frequency)). The impact of these variations in the analytical model results was verified, and therefore, the L_m and R_r parameters had a high impact in the model accuracy, while the variation of the remaining parameters is almost insignificant. Related to this analysis, the impact of choosing the wrong capacitor values can cause the overload of the SEIG or the non-excitation of it. This is crucial, since these values are significant when the flow and head in the water systems change as a consequence of the variability of the demand, and therefore, the PAT+SEIG system has to be adjusted to the rotational speed continuously, in order to maximize the recovered energy.

The incorporation of the parameters variation in the analytical model increased its accuracy, reducing the error between analytical and experimental results from 50.8%, with fixed parameters, to 13.2% considering all parameters changing. This reduction enabled to get a better approximation of the capacitance required to self-excite and maximize the SEIG output power, for each rotational speed and load, being possible, under optimal conditions, to increase the overall peak efficiency of the PAT-SEIG system from 26% to 40%. Note that this study was done for a low power SEIG with a low rated electrical efficiency of 68% which, along with the maximum PAT efficiency of around 60%, resulted in low overall efficiency of 40%. For higher power SEIG, the electrical efficiency is much higher.

The development of this methodology has a great impact in the strategies of the efficiency improvement in the water systems since the method enabled to know the variability of the overall efficiency as a function of the rotational speed of the hydraulic machine. Therefore, considering the new future research lines in the improvement of the water-energy nexus, the incorporation of this methodology can be used in the real cases in order to know the effective efficiency when the machine operates in "off-grid". Besides, the use of this methodology will allow water managers to choose the hydraulic machine as a function of the hydraulic characteristic and the electric machine (PAT + SEIG) that considers the available recovery points. This consideration is of utmost importance to choose the best hydraulic machine and the best inductor motor to maximize the overall efficiency since the inductor proposed by the manufacturer to be connected to the grid is not always the best to operate in "off-grid"

Acknowledgments:

This work was supported by FCT, through IDMEC, under LAETA, project UID/EMS/50022/2013 and the project REDAWN (Reducing Energy Dependency in Atlantic Area Water Networks) EAPA_198/2016 from INTERREG ATLANTIC AREA PROGRAMME 2014-2020 and CERIS (CEHIDRO-IST), the Hydraulic Laboratory, for experiments on PATs.

Conflicts of Interest:

The authors declare no conflict of interest.

The founding sponsors had no role in the design of the study; in the collection, analyses, or interpretation of data; in the writing of the manuscript, and in the decision to publish the results.

5 REFERENCES

[1] Şiir Kılkış, Goran Krajačić, Neven Duić, Marc A. Rosen, Moh'd Ahmad Al-Nimr, "Advancements in sustainable development of energy, water and environment systems", Energy Conversion and Management, 176, 2018, Pages 164-183. doi: 10.1016/j.enconman.2018.09.015.

[2] Ramos, H., Borga, A., "Pumps as turbines: an unconventional solution to energy production". Urban Water 1, 261–263. doi: 10.1016/S1462-0758(00)00016-9.

[3] S. Barbarelli, M. Amelio, G. Florio, "Experimental activity at test rig validating correlations to select pumps running as turbines in microhydro plants", Energy Conversion and Management, 149, 2017, pp. 781-797, https://doi.org/10.1016/j.enconman.2017.03.013.

[4] Mateus Ricardo Nogueira Vilanova, José Antônio Perrella Balestieri, "Hydropower recovery in water supply systems: Models and case study", Energy Conversion and Management, 84, 2014, pp. 414-426, https://doi.org/10.1016/j.enconman.2014.04.057.

[5] Williams, A.A. "Pumps as turbines for low cost micro hydro power". Renew. Energy, 9, 1999, 1227–1234. doi: 10.1016/0960-1481(96)88498-9.

[6] Daniele Novara, Aonghus McNabola, "A model for the extrapolation of the characteristic curves of Pumps as Turbines from a datum Best Efficiency Point", Energy Conversion and Management, 174, 2018, pp. 1-7, https://doi.org/10.1016/j.enconman.2018.07.091.

[7] Binama, M., Su, W.-T., Li, X.-B., Li, F.-C., Wei, X.-Z., An, S., 2017. Investigation on pump as turbine (PAT) technical aspects for micro hydropower schemes: A state-of-the-art review. Renew. Sustain. Energy Rev. 79, 148–179. doi: 10.1016/J.RSER.2017.04.071.

[8] Samora, I.; Franca, M.; Schleiss, A.; Ramos, H.M. "Simulated Annealing in Optimization of Energy Production in a Water Supply Network". *Water Resour. Manag*. 2016, vol. 30, pp. 1533–1547. doi: 10.1007/s11269-016-1238-5.

[9] Samora, I.; Manso, P.; Franca, M.J.; Schleiss, A.J.; Ramos, H.M. "Energy Recovery Using Micro-Hydropower Technology in Water Supply Systems: The Case Study of the City of Fribourg". Water 2016, 8(8), 344; https://doi.org/10.3390/w8080344.

[10]Pérez-Sánchez, Modesto; Sánchez-Romero, Francisco-Javier; Helena M. Ramos; López Jiménez, Petra Amparo. "Modeling Irrigation Networks for the Quantification of Potential Energy Recovering: A Case Study". *Water*, 2016, vol. 8, pp. 1 - 26. doi: 10.3390/w8060234.

[11]Fontana N, Giugni M, Portolano D, "Losses reduction and energy production in water-distribution networks". *J Water Res Pl-ASCE*, 2012, 138(3), pp. 237–244.

[12] Capelo, B., Pérez-Sánchez, M., Fernandes, J.F.P., Ramos, H.M., López-Jiménez, P.A., Branco, P.J.C. "Electrical behaviour of the pump working as turbine in off grid operation". Appl. Energy 208, 302–311. doi: 10.1016/J.APENERGY.2017.10.039.

[13] Mandelli, S., Barbieri, J., Mereu, R., & Colombo, E. (2016). Off-grid systems for rural electrification in developing countries: Definitions, classification and a comprehensive literature review. Renewable and Sustainable Energy Reviews, 2016, vol. 58, pp. 1621-1646. doi: 10.1016/j.rser.2015.12.338

[14] Rossi, M., Righetti, M., Renzi, M. "Pump-as-turbine for Energy Recovery Applications: The Case Study of An Aqueduct". Energy Procedia 2016, 101, 1207–1214. doi: 10.1016/J.EGYPRO.2016.11.163.

[15] A. Carravetta, S. Derakhshan, H. M. Ramos. "Pumps as Turbines, Fundamentals and Applications". Springer International Publishing, ISSN 2195-9862, 2018. Doi: 10.1007/978-3-319-67507-7.

[16] Braga, A.V., Rezek, A.J.J., Silva, V.F., Viana, A.N.C., Bortoni, E.C., Sanchez, W.D.C., Ribeiro, P.F.. "Isolated induction generator in a rural Brazilian area: Field performance tests". Renew. Energy 2015 83, 1352–1361. doi: 10.1016/J.RENENE.2015.05.057.

[17] S.N. Mahato, S.P. Singh, M.P. Sharma, “Excitation capacitance required for self excited single phase induction generator using three phase machine”, Energy Conversion and Management, 49, 5, 2008, pp. 1126-1133, https://doi.org/10.1016/j.enconman.2007.09.007.

[18] Khan, M. F. and Khan, M. R., "Self regulating three phase-self excited induction generator for standalone generation," 2013 Annual IEEE India Conference (INDICON), Mumbai, 2013, pp. 1-6. doi: 10.1109/INDCON.2013.6726124.

[19] Nigim , K.A., Salama , M.M.A., Kazerani, M. “Identifying machine parameters influencing the operation of the self-excited induction generator”. Electric Power Systems Research, 2004, vol. 69, p. 123-128. doi: 10.1016/j.epsr.2003.08.003.

[20] Khan, S., Shadzad, M., Palensky, P. and Jahangir, K., "Dynamics of wind-turbine driven Self-Excited Induction Generator with online parameter calculation," IECON 2013 - 39th Annual Conference of the IEEE Industrial Electronics Society, Vienna, 2013, pp. 5271-5275. doi: 10.1109/IECON.2013.6699992.

[21] Eltamaly, Ali M. "New formula to determine the minimum capacitance required for self-excited induction generator." Power Electronics Specialists Conference, 2002. PESC 02. 2002 IEEE 33rd Annual. vol. 1. Doi: 10.1109/PSEC.2002.1023854.

[22] Mahajan, S. M., Kumar, S. S., Kumaresan, N., Gounden, N. G. A., Rajkumar, E., “Decoupled control strategy for the operation of capacitor-excited induction generator for DC power applications”, IET Power Electronics, 2016, vol. 9, pp. 2551 – 2561, doi: 10.1049/iet-pel.2015.0830.

[23] Radić, M. , Stajić, Z., Floranović, N., “Performance Characteristics Of A Three-Phase Self-Excited Induction Generator Driven By Regulated Constant Speed Turbine”, Automatic Control and Robotics, 2012, vol. 11, n.1, pp. 57-67.

[24] Simao, M; Pérez-Sánchez, Modesto; Carraveta; López Jiménez, Petra Amparo; Helena M. Ramos. “Velocities in a Centrifugal PAT Operation: Experiments and CFD Analyses”. Fluids, 2018, 3 (3), 1 - 21. 10.3390/fluids3010003.

Annex

A.1 Coefficients D_i of equation (13)

$$D_6 = X_m{}^2 X_r{}^2 \Big(\big(R_s + R_m\big) X_L{}^2 + R_L X_s{}^2\Big) \tag{A-1}$$

$$D_5 = -2X_m{}^2 b X_r{}^2 \Big((R_s + R_m) X_L{}^2 + R_L X_s{}^2\Big) \tag{A-2}$$

$$\begin{aligned} D_4 = &\Big\{ R_r{}^2 (R_L X_s{}^2 + R_s X_L{}^2) + \Big[(X_L{}^2 b^2 + R_L{}^2 + 2R_L R_s) X_r{}^2 + 2R_r \Big(R_L X_s{}^2 + \frac{1}{2} X_L{}^2 (R_r + 2R_s) \Big)\Big] R_m + \\ &+ \Big(R_L (X_s + X_r)^2 + X_L{}^2 (R_r + R_s) \Big) R_m{}^2 + \Big(R_L (R_L R_S + X_S{}^2 b^2 + R_s{}^2) + b^2 R_s X_L{}^2 \Big) X_r{}^2 \Big\} X_m{}^2 + \\ &+ 2R_m{}^2 X_r (R_L X_r X_s + R_L X_s{}^2 + R_s X_L{}^2) X_m + X_r{}^2 (R_L X_s{}^2 + R_s X_L{}^2) R_m{}^2 \end{aligned} \tag{A-3}$$

$$\begin{aligned} D_3 = -2b &\Big\{ \Big[\Big((X_r + X_s)^2 R_L + \frac{1}{2} X_L{}^2 (R_r + 2R_s) \Big) X_m{}^2 + 2X_r X_m \Big(R_L (X_s X_r + X_s{}^2) + R_s X_L{}^2 \Big) + \\ &+ X_r{}^2 (R_L X_s{}^2 + R_s X_L{}^2) \Big] R_m{}^2 + \Big(R_L{}^2 X_r{}^2 + (R_r X_s{}^2 + 2R_s X_r{}^2) R_L + R_r R_s X_L{}^2 \Big) X_m{}^2 R_m + R_L R_s X_m{}^2 X_r{}^2 (R_L + R_s) \Big\} \end{aligned} \tag{A-4}$$

$$\begin{aligned} D_2 = &\Big\{ \Big[\Big((X_r + X_s)^2 b^2 + (R_r + R_s)^2 \Big) X_m{}^2 + \Big(2R_s{}^2 X_r + 2X_s (X_r{}^2 b^2 + X_r X_s b^2 + R_r{}^2) \Big) X_m + R_s{}^2 X_r{}^2 + \\ &+ X_s{}^2 (X_r{}^2 b^2 + R_r{}^2) \Big] R_m{}^2 + 2R_s X_m{}^2 (X_r{}^2 b^2 + R_r{}^2 + R_r R_s) R_m + R_s{}^2 X_m{}^2 (X_r{}^2 b^2 + R_r{}^2) \Big\} R_L + \\ &+ R_m{}^2 R_s X_L{}^2 \Big((X_m X_r)^2 b^2 + R_r{}^2 \Big) + \Big[R_m{}^2 \Big((R_r + R_s) X_m{}^2 + 2R_s X_r X_m + R_s X_r{}^2 \Big) + \\ &+ X_m{}^2 \Big(R_m (X_r{}^2 b^2 + R_r{}^2 + 2R_r R_s) + R_s (X_r{}^2 b^2 + R_r{}^2) \Big) \Big] R_L{}^2 \end{aligned} \tag{A-5}$$

$$\begin{aligned} D_1 = -R_m R_L b &\Big\{ \Big[2(X_m + X_r)^2 R_s{}^2 + \Big((2R_L + 2R_r) X_m{}^2 + 4R_L X_r X_m + 2R_L X_r{}^2 \Big) R_s + R_L R_r X_m{}^2 \Big] R_m \\ &+ 2R_r R_s X_m{}^2 (R_L + R_s) \Big\} \end{aligned} \tag{A-6}$$

$$D_0 = R_m{}^2 R_L R_s (R_L + R_s) \Big((X_m + X_r)^2 b^2 + R_r{}^2 \Big) \tag{A-7}$$

A.2 Coefficients A_i and B_i of equation (14)

$$A_8 = X_L{}^2 X_m{}^2 X_r{}^2 X_s{}^2 \tag{A-8}$$

$$A_7 = -2X_L^2 X_m^2 X_r^2 X_s^2 b \tag{A-9}$$

$$\begin{aligned} A_6 = &\Big\{\Big[\Big(b^2 X_s^2 + (R_m + R_s)^2\Big) X_r^2 + 2R_m^2 X_r X_s + X_s^2 (R_m + R_r)^2\Big] X_m^2 + 2R_m^2 X_r X_s X_m (X_r + X_s) + \\ &+ R_m^2 X_r^2 X_s^2\Big\} X_L^2 + R_L^2 X_m^2 X_r^2 X_s^2 \end{aligned} \tag{A-10}$$

$$\begin{aligned} A_5 = &-2b\Big\{\Big[\Big((X_r + X_s)^2 R_m^2 + (R_r X_s^2 + 2R_s X_r^2) R_m + R_s^2 X_r^2\Big) X_m^2 + 2R_m^2 X_r X_s (X_r + X_s) X_m + \\ &+ R_m^2 X_r^2 X_s^2\Big] X_L^2 + R_L^2 X_m^2 X_r^2 X_s^2\Big\} \end{aligned} \tag{A-11}$$

$$\begin{aligned} A_4 = &2R_m^2 X_m \Big[\Big(b^2 X_r^2 X_s + (X_s^2 b^2 + R_s^2) X_r + R_r^2 X_s\Big) X_L^2 + R_L^2 X_r X_s (X_r + X_s)\Big] + \\ &X_m^2 \Big\{R_m^2 \Big[\Big(b^2 (X_r + X_s)^2 + (R_r + R_s)^2\Big) X_L^2 + R_L^2 (X_r + X_s)^2\Big] + R_m \Big[2R_s X_L^2 \Big(b^2 X_r^2 + R_r (R_r + R_s)\Big) + \\ &+ 2R_L^2 (R_r X_s^2 + R_s X_r^2)\Big] + R_s^2 (X_r^2 b^2 + R_r^2) X_L^2 + R_L^2 \Big((X_s^2 b^2 + R_s^2) X_r^2 + X_s^2 R_r^2\Big)\Big\} + \\ &+ R_m^2 \Big[\Big((X_s^2 b^2 + R_s^2) X_r^2 + X_s^2 R_r^2\Big) X_L^2 + R_L^2 X_r^2 X_s^2\Big] \end{aligned} \tag{A-12}$$

$$\begin{aligned} A_3 = &-2b\Big\{\Big[\Big(R_L^2 (X_r + X_s)^2 + R_s X_L^2 (R_r + R_s)\Big) X_m^2 + 2X_r X_m \Big(X_s (X_r + X_s) R_L^2 + R_s^2 X_L^2\Big) + \\ &+ X_r^2 (R_L^2 X_s^2 + R_s^2 X_L^2)\Big] R_m^2 + \Big((R_r X_s^2 + 2R_s X_r^2) R_L^2 + R_r R_s^2 X_L^2\Big) X_m^2 R_m + R_L^2 R_s^2 X_m^2 X_r^2\Big\} \end{aligned} \tag{A-13}$$

$$\begin{aligned} A_2 = &\Big\{\Big[\Big((X_r + X_s)^2 b^2 + (R_r + R_s)^2\Big) X_m^2 + \Big(2R_s^2 X_r + 2X_s (X_r^2 b^2 + X_r X_s b^2 + R_r^2)\Big) X_m + R_s^2 X_r^2 + \\ &+ + X_s^2 (X_r^2 b^2 + R_r^2)\Big] R_L^2 + R_s^2 X_L^2 \Big((X_m + X_r)^2 b^2 + R_r^2\Big)\Big\} R_m^2 + R_L^2 R_s^2 X_m^2 (X_r^2 b^2 + R_r^2) + \\ &+ 2R_L^2 R_s X_m^2 R_m (X_r^2 b^2 + R_r^2 + R_r R_s) \end{aligned} \tag{A-14}$$

$$A_1 = -2R_m R_L^2 R_s b \Big[\Big((X_m + X_r)^2 R_s + X_m^2 R_r\Big) R_m + R_r R_s X_m^2\Big] \tag{A-15}$$

$$A_0 = R_m^2 R_L^2 R_s^2 \Big((X_m + X_r)^2 b^2 + R_r^2\Big) \tag{A-16}$$

$$B_6 = X_L^2 X_m^2 X_r^2 X_s + X_L X_m^2 X_r^2 X_s^2 \tag{A-17}$$

$$B_5 = -2X_L X_m^2 X_r^2 X_s b (X_L + X_s) \tag{A-18}$$

$$\begin{aligned}B_4 = &\Big[\big((X_r^2 b^2 + R_m^2 + 2R_m R_r + R_r^2) X_s + R_m^2 X_r\big) X_m^2 + R_m^2 X_r (X_r + 2X_s) X_m + R_m^2 X_r^2 X_s\Big] X_L^2 \\ &+\Big[\Big(\big(X_r^2 b^2 + (R_m + R_r)^2\big) X_s^2 + 2R_m^2 X_r X_s + (R_m + R_s)^2 X_r^2\Big) X_m^2 + 2R_m^2 X_r X_s (X_r + X_s) X_m + \\ &+ R_m^2 X_r^2 X_s^2\Big] X_L + R_L^2 X_m^2 X_r^2 X_s\end{aligned} \tag{A-19}$$

$$\begin{aligned}B_3 = -2b\Big\{&R_m X_L^2 \Big[(X_m + X_r)\big((X_r + X_s) X_m + X_r X_s\big) R_m + R_r X_m^2 X_s\Big] + R_L^2 X_m^2 X_r^2 X_s + \\ &+\Big[\big((X_r + X_s) X_m + X_r X_s\big)^2 R_m^2 + (R_r X_s^2 + 2R_s X_r^2) X_m^2 R_m + R_s^2 X_m^2 X_r^2\Big] X_L\Big\}\end{aligned} \tag{A-20}$$

$$\begin{aligned}B_2 = &\Big\{\Big[b^2 (X_r + X_s) X_L^2 + \big(b^2 X_r^2 + 2b^2 X_r X_s + b^2 X_s^2 + (R_r + R_s)^2\big) X_L + R_L^2 (X_r + X_s)\Big] X_m^2 + \\ &+\Big[\big(b^2 X_r^2 + 2X_r X_s b^2 + R_r^2\big) X_L^2 + \big(2X_r^2 X_s b^2 (X_r + X_s) + 2(R_s^2 X_r + R_r^2 X_s)\big) X_L + \\ &+ R_L^2 X_r (X_r + 2X_s)\Big] X_m + X_s (X_r^2 b^2 + R_r^2) X_L^2 + \big((X_s^2 b^2 + R_s^2) X_r^2 + R_r^2 X_s^2\big) X_L + R_L^2 X_r^2 X_s\Big\} R_m^2 + \\ &+ 2X_m^2 R_m \Big[\big(b^2 X_r^2 + R_r (R_r + R_s)\big) R_s X_L + R_L^2 R_r X_s\Big] + X_m^2 (X_r^2 b^2 + R_r^2)(R_L^2 X_s + R_s^2 X_L)\end{aligned} \tag{A-21}$$

$$\begin{aligned}B_1 = -2R_m b\Big\{&\Big[\big(R_L^2 (X_r + X_s) + R_s X_L (R_r + R_s)\big) X_m^2 + X_r X_m \big((X_r + 2X_s) R_L^2 + 2R_s^2 X_L\big) + \\ &+ X_r^2 (R_L^2 X_s + R_s^2 X_L)\Big] R_m + R_r X_m^2 (R_L^2 X_s + R_s^2 X_L)\Big\}\end{aligned} \tag{A-22}$$

$$\begin{aligned}B_0 = R_m^2 \Big\{&(X_m + X_r) b^2 \Big[\big((X_r + X_s) X_m + X_r X_s\big) R_L^2 + R_s^2 X_L (X_m + X_r)\Big] + \\ &+ R_r^2 \big((X_m + X_s) R_L^2 + R_s^2 X_L\big)\Big\}\end{aligned} \tag{A-23}$$